Response to Referee Comments for Manuscript amt-2020-217

Referee #1:

The manuscript presents low-cost air quality sensor unit for multipollutant, including toxic gases, particulate matter and greenhouse gases (carbon dioxide and methane). The authors report detailed characterisation of two variants of the device: stationary and portable version and present some preliminary results from few field studies. In addition to the characterising the devices, the authors present an online calibration method that rely on the use of traceable gas which is incorporated into the device with auto-calibration functionality built into the operational software of device. This manuscript is well written and presents a new approach physical calibration approach that is more comprehensive than any other work in this field of low-cost air quality sensor. The manuscript also present recommendations on best practices related to design, characterising and deployment of this type of device.

- The authors did not address the issue of safety for the online calibration system which relies on the use of pressurised calibration cylinder (1500 psig). Under normal ambient application, the static variant of the multipollutant device may be exposed to high temperatures especially in the summer. This could pose potential safety concern for the structural integrity of the device.

Response: *Thank you for identifying this missing element in the text. It was however something we considered extensively in the design of the device. The cylinder, valves, and associated fittings are selected based on their specifications to withstand the cylinder pressure (reference: Swagelok/TESCOM specifications). For example, the pressurized gas calibration cylinder is constructed with 304L stainless steel with a DOT-3E1800 specification. This specification allows for a maximum working pressure of 1800 psig between -53°C to 37°C, which is higher than our use of 1500 psig. Elevated summertime temperatures are indeed one consideration. The specification calls for a maximum working pressure of 1360 psig at a temperature of 93°C, but based on summertime temperatures in our testing, the monitors do not go over 60°C, and best monitor siting practices suggests shading of the monitor to further mitigate elevated temperatures (as discussed in Section 3.6).*

We have added text to the manuscript (lines 251-256) to address this point, and instruct future researchers to pay attention to component specifications and the standard gas concentrations in the cylinder. Furthermore, labels within the device are also used to warn users about the presence of pressurized gas.

- The authors have reported using B431 Alphasense sensor for the OX (P. 3, line 93) but the Table 1 and the text in line 90 page 3 suggest a variant was used. In addition, the authors stated that the static variant uses MiCS-2614 for O3, does this mean the static and portable unit has both OX and O3 measurements? The authors need to clarify this ambiguity.

Response: *In the manuscript, the stationary version of the monitor uses the MiCS-2614 sensor to measure O_3 while the portable monitor uses the Alphasense A431 sensor to measure O_3. (via the NO_2 subtraction specified by Alphasense). However, the 3D printed gas manifold was designed to be able to accommodate*

the Alphasense A431 sensor in the stationary monitor if necessary given the uniform size of the Alphasense A-series sensors. For this study, the Alphasense A431 sensor was solely used in the portable monitor. To reduce any confusion or ambiguity, we have removed the O_x listing on line 93 and added a column to Table 1 to specify which sensors are used in each version.

- I recommend the authors annotate figure 1(b) and figure S3 (a & b) with labels showing main components of the photo presented.

Response: Thank you for the suggestion. We have added annotations for the main components (e.g. gas inlet, online calibration cylinder) in Figure 1 and Figure S3.

- P. 10, line 297, the phrase ". . .by the Plantower sensor" sound like the authors are referring to the reference device rather than the MPM device Suggest something like ". . .. . .by the multipollutant device collocated with the reference at the Baltimore Oldtown"

Response: Thank you for the comment, we have changed the wording to be less ambiguous.

- P. 17, line 491: there is a red font in the text.

Response: Fixed, thank you.

- P. 17, line 494: remove the "of" in the sentence.

Response: Fixed, thank you.

- P. 23, line 625 (Figure 3 (a)) add the RH/T corrected to the legend of the time series. Ditto for figures 4(a) and 5(a)

Response: We have added language to the caption to indicate that "Our Monitor" in the (a) panel time series for Figures 3, 4, and 5 is the corrected, not raw, data.

- P. 25, figure 8 and 9 captions should include the dates for this deployment.

Response: We have added the deployment dates in the captions of figure 8 and 9. The NYC deployment occurred on June 23rd, 2018 and the Baltimore deployment occurred on March 2nd, 2019.

- P. 4, line 85, the phrase ". . . Eqn S2 and Eqn S3" should read ". . . Eqn S3 and Eqn S4"

Response: Fixed, thank you.

- P. 9, Figure S9 caption should include the temperature range for the two plots (< 18 and > 18 degree C).
Response: Fixed, thank you.

Referee #2:

This manuscript presents the design of a new low-cost sensor system that incorporates an innovative approach to maintaining sensor performance – an automated system for performing zero/span calibrations. This manuscript is particularly relevant as the integration of a zero/span system into a low-cost sensor device has the potential to help address the ongoing challenges of sensor drift and degradation. The authors provide a detailed description of the technology, including the sensors incorporated as well as the hardware and software. Two versions of the device have been created to accommodate stationary and portable monitoring. The authors also share initial results on performance of the device and compare these results to previous studies.

- Multiple studies have observed that calibrating sensors using field co-location data as opposed to a laboratory approach tends to result in higher performing and more robust calibrations (e.g., the study mentioned in lines 56-57). Considering this information, it is recommended that the authors discuss their rationale for using a laboratory calibration approach (lines 200 -201). In addition, do the authors anticipate any limitations regarding the zero/span system given that the span gas will not have the same mixture of background pollutants as the ambient air being sampled?

Response: *We agree with the reviewer that field co-location is a very effective approach to sensor calibration. In fact, in the larger project that uses the monitors described in this study, we employ a hybrid approach to calibration that utilizes co-location as part of the strategy. As noted in Section S1, we use laboratory calibrations to get initial sensor calibration and quality control performance, as well as develop field environmental correction factors with each type of sensor for relative humidity and temperature (where appropriate) that build off of the laboratory calibrations. For example, in a recent paper we employ co-location approaches to develop a statistical calibration method for the $PM_{2.5}$ sensor used in our multipollutant monitor (Datta et al., 2020; Atoms. Env., doi: 10.1016/j.atmosenv.2020.117761). The on-board system is designed for future longer deployments to maintain better calibrations and track sensor response/zero drift during the in-field period after lab calibration and/or co-location with reference monitors. A few limitations of the zero/span system described in the paper are the number of reactive gases one can effectively combine into a single standard mixture and the available materials for room temperature removal of pollutants in the zero trap. Another limitation is the potential for insufficient cylinder pressure as the tank approaches empty, which can be tracked by instillation date and calibration frequency, as well as monitoring calibration data. At current rates the cylinder can operate for over a year before needing to be refilled. Other limitations are addressed by maintaining acceptable relative humidity during the zero and span functions (e.g. water permeation setup) and using variable calibration schedules to get variations in calibration temperature. Additionally, the online data visualization platform we utilize (Grafana) also allows us to remotely monitor calibrations and replace poorly performing monitors in near real time. Without this, we would need to wait until the deployment ended to check for monitor performance. We acknowledge that the*

background mixture is going to be different during the span checks (less so during the zero check), but that is not unlike calibration with typical instruments/standards, and has the advantage of reducing confounding factors that could introduce additional variables that would affect the ability to track drift over time. To address the reviewer's comment we have examined and revised relevant sections of the text to ensure this discussion is accurately reflected (Section 2.1.4).

- On line 67 the authors mention the issue of sensor drift – given the wide range of sensor types used, it is recommended that the authors expand this discussion to include how drift and cross-sensitivities tend to vary by sensor type.

Response: We agree that understanding sensor drift and cross-sensitivities to other pollutants are key for low cost sensor deployment. To address the reviewer's request, we have added a couple sentence summary in the sensor methods section and referenced a more comprehensive review of low-cost air quality sensors from the World Meteorological Organization which includes discussion of sensor drift and common cross-sensitivities (in the introduction at line 66-68 and in the Section 2.1.1).

- Regarding the modification to the Figaro 2600, according to the results in Figure S6 – even though the trends are linear, it appears that adding the charcoal filter seems to reduce the sensor's sensitivity, are there any other impacts from this modification, such as a slowed response time? Recommend adding more discussion on this topic.

Response: As noted in the reviewer's comment, the use of the activated carbon filter slightly reduced the total sensor response (while remaining linear) to CH_4 concentrations tested in the 1.4-2.4 ppm range, which may be attributed to decreases in background VOCs. It is possible that there may be a very slight increase in sensor response time due to the added diffusion length for gases, but that was not observed here and is not expected to be an issue with minute resolution data averages. To ensure that accurate response factors are generated in conditions similar to ambient measurements, all calibrations are performed with the activated carbon filter in place. In Section 2.1.3 we discuss these and other potential issues arising from the use of using the charcoal filter. For example, we implement a 3D-printed PLA shell to keep the filter in place which could react with pollutants of interest (e.g. ozone). Teflon "tape" is placed around the filter in order to reduce interactions between the shell and reactive gases as well as prevent any charcoal fibers from shedding the inside the gas manifold.

- Were the portable monitors also tested via a co-location in the field with reference instruments, if not could the authors discuss the rationale?

Response: For this study, the portable monitors were not co-located in the field since they largely consist of the same sensors (exception: Alphasense Ox sensor) and a similar physical design that was scaled down. We focused evaluation efforts on the stationary multipollutant monitor that had a larger set of sensors, which are included as part of the portable monitor. It was not viewed as necessary to co-locate the portable configuration as well, especially considering it is not constructed with the same extent of

weatherproofing. In the manuscript we focus on $PM_{2.5}$ as a proof of concept for high spatiotemporal personal exposure studies which uses the same Plantower sensor used in the stationary model.

- In Section 3.4, the authors discuss the performance of the zero/span system. It is recommended that the authors comment on the impact of the system on sensor performance for each pollutant. During the field co-location tests, did the implementation of the system have any clear impact on the resulting data? It seems this system might be most useful during long-term deployments - though the field tests appear to range between 1 week to 1 month long.

Response: We agree with reviewer that this is an interesting area for ongoing work and evaluation of the system and that it will be most useful for longer-term deployments (e.g. months to 1+ year) where drift with sensor aging will be more pronounced. Unfortunately, given the duration of the measurements used in this manuscript, we are unable to include this additional analysis/discussion, but we have added that future work in the field should examine the effect of on-board calibration systems on long-term sensor performance. We have updated language in Section 2.1.4 to address this concern.

- In Section 3.5, for Table 3, it is recommended that the authors add columns or a second table that lists the length of the deployment, the location of the deployment, and the calibration approach used (i.e., field or lab). In addition, consider highlighting C2 or adding comparisons to results for which a laboratory calibration was tested in the field.

Response: We agree that the length of deployment and location of deployment is of great importance when comparing between low cost sensors. We have broken up Table 3 into two tables now to allocate additional space for deployment length and deployment location. Additionally, two additional studies have been added to the comparison (the Berkeley Atmospheric CO_2 Observation Network). Language related to this addition has been updated in Section 3.5 (Comparison with Literature).

- In Section 3.5, in Table 3, for all pollutants except PM2.5 the raw OEM sensors are listed, whereas the names of commercial devices are listed for PM2.5 – recommend adding the raw OEM sensor used for all devices.

Response: Thank you for the suggestion, we have updated to include OEM sensor data where appropriate in Table 4.

- Reconsider the use of the term 'monitor' throughout the manuscript (i.e., multipollutant monitor and portable monitor). These devices are typically referred to as a sensor, sensor platform, or sensor system, while generally the term monitor is reserved for research or regulatory grade instruments.

Response: We appreciate the reviewer's attention to word choice. To avoid confusion, we deliberately used the term "monitor" in the manuscript to represent the collection of various sensors together in one "multipollutant monitor" along with all of the other components (e.g. flow and calibration systems) and use the term "sensor" to refer to the individual sensing components (e.g. electrochemical sensor, optical

sensor) which have their own dedicated sections. This was done to represent the device as a collection of a wide range of different sensor types and suppliers, and not to suggest that there is a single sensing component measuring all the pollutants listed. Based on a survey of other papers, popular devices and the language used to describe them on the AQMD AQ-Spec and EPA Air Sensor Toolbox, the terms monitor and sensor are used somewhat interchangeably to describe the overall devices (e.g. ELM monitor, Aeroqual monitor) and the term "reference monitor" is used elsewhere to describe the regulatory instruments they are compared to. For example, in Atmospheric Measurement Techniques there have been several recent articles which use the term "monitor" in the same manner as in this paper. In Malings et al. (2019) *the researchers developed a "Real-time Affordable Multi-Pollutant (RAMP) monitor" comprised of low cost sensors similar to those in our multipollutant monitor. Another example comes from* Wendt et al. (2019)*, who design a low cost monitor for measuring $PM_{2.5}$ and aerosol optical depth (AOD). Yet, we do acknowledge these the term "sensor" is typically used to describe low-cost non-regulatory methods, and we do not intend to misrepresent the devices as federal reference methods. To address the reviewer's comment we have added the following language in the introduction to clarify the word choice at the outset: "Here the term "monitor" or "multipollutant monitor" is used to describe the collection of sensors and other components (e.g. flow channels, valves, online calibration system) used while the term "sensor" is used to describe the standalone sensing components. " (Section 2.1.1, lines 76-78).*

References:

Malings, C., Tanzer, R., Hauryliuk, A., Kumar, S. P. N., Zimmerman, N., Kara, L. B., Presto, A. A. and Subramanian, R.: Development of a general calibration model and long-term performance evaluation of low-cost sensors for air pollutant gas monitoring, Atmos. Meas. Tech., 12(2), 903–920, doi:10.5194/amt-12-903-2019, 2019.

Wendt, E. A., Quinn, C. W., Miller-Lionberg, D. D., Tryner, J., L'Orange, C., Ford, B., Yalin, A. P., Jeffrey, P., Jathar, S. and Volckens, J.: A low-cost monitor for simultaneous measurement of fine particulate matter and aerosol optical depth - Part 1: Specifications and testing, Atmos. Meas. Tech., 12(10), 5431–5441, doi:10.5194/amt-12-5431-2019, 2019.

- There is some red text on line 491.

<u>Response:</u> *Fixed, thank you.*

Stationary and Portable Multipollutant Monitors for High Spatiotemporal Resolution Air Quality Studies including Online Calibration

Colby Buehler[1,2], Fulizi Xiong[1,2], Misti Levy Zamora[2,3], Kate M. Skog[1], Joseph Kohrman-Glaser[4], Stefan Colton[4], Michael McNamara[5], Kevin Ryan[5], Carrie Redlich[6,7], Matthew Bartos[8], Brandon Wong[8], Branko Kerkez[8], Kirsten Koehler[2,3], Drew R. Gentner[1,2,9,*]

[1] Department of Chemical & Environmental Engineering, Yale University, School of Engineering and Applied Science, New Haven, Connecticut 06511, USA

[2] SEARCH (Solutions for Energy, Air, Climate and Health) Center, Yale University, New Haven, CT, USA

[3] Department of Environmental Health and Engineering, Johns Hopkins Bloomberg School of Public Health, Baltimore, MD, 21205, USA

[4] Department of Mechanical Engineering, Yale University, School of Engineering and Applied Science, New Haven, Connecticut, 06511, USA

[5] Department of Electrical Engineering, Yale University, School of Engineering and Applied Science, New Haven, Connecticut, 06511, USA

[6] Department of Internal Medicine, Yale University, School of Medicine, New Haven, Connecticut, 06510, USA

[7] Department of Environmental Health Sciences, Yale University, School of Public Health, New Haven, Connecticut, 06511, USA

[8] Civil and Environmental Engineering, University of Michigan, 2350 Hayward St, G.G. Brown Building, Ann Arbor, MI 48109, USA

[9] Max Planck Institute for Chemistry, Mainz 55128, Germany.

Correspondence to: Drew R. Gentner (drew.gentner@yale.edu)

Abstract. The distribution and dynamics of atmospheric pollutants are spatiotemporally heterogeneous due to variability in emissions, transport, chemistry, and deposition. To understand these processes at high spatiotemporal resolution and their implications for air quality and personal exposure, we present custom, low-cost air quality monitors that measure concentrations of contaminants relevant to human health and climate, including gases (e.g. O_3, NO, NO_2, CO, CO_2, CH_4, and SO_2) and size-resolved (0.3–10 µm) particulate matter. The devices transmit sensor data and location via cellular communications, and are capable of providing concentration data down to second-level temporal resolution. We produce two models; one designed for stationary (or mobile platform) operation, and a wearable, portable model for directly measuring personal exposure in the breathing zone. To address persistent problems with sensor drift and environmental sensitivities (e.g. relative humidity and temperature), we present the first online calibration system designed specifically for low-cost air quality sensors to calibrate zero and span concentrations at hourly to weekly intervals. Monitors are tested and validated in a number of environments across multiple outdoor and indoor sites in New Haven, CT, Baltimore, MD, and New York City. The

evaluated pollutants (O_3, NO_2, NO, CO, CO_2, and $PM_{2.5}$) performed well against reference instrumentation (e.g. r=0.66–0.98) in urban field evaluations with fast e-folding response times (≤ 1 min), making them suitable for both large-scale network deployments and smaller-scale targeted experiments at a wide range of temporal resolutions. We also provide a discussion of best practices on monitor design, construction, systematic testing, and deployment.

1 Introduction

Exposures to air pollution are associated with elevated health risks such as cardiorespiratory inflammatory responses and oxidative stress (Brauer et al., 2012; Chuang et al., 2007; Pope and Dockery, 2006). Each year outdoor air pollution leads to approximately 4.2 million premature deaths worldwide and is the fifth highest mortality risk factor in the Global Burden of Disease Study 2015 (Cohen et al., 2017; Forouzanfar et al., 2016). Assessment of public health risks and regulatory standards requires accurate measurement of air pollution levels. However, traditional analytical techniques for air pollutant measurements—such as spectroscopy, chemiluminescence, and mass spectrometry—are expensive, which limits the deployment of instruments to sparsely-located state and federal air quality monitoring sites and targeted research campaigns. As a result, the spatiotemporal variations in urban human exposure caused by localized combustion sources (e.g. motor vehicles, cooking) and other sources are not well understood (Kheirbek et al., 2013).

The need for better geospatial coverage in air quality monitoring has resulted in multiple studies that utilize low-cost sensors to measure a range of pollutants in portable and stationary configurations (e.g., Bigi et al., 2018; Castell et al., 2017; Cross et al., 2017; Hagan et al., 2018; Kim et al., 2018; Lewis et al., 2016; Mead et al., 2013; Popoola et al., 2016; Thorson et al., 2019; Zimmerman et al., 2018). Wearable devices containing sensors to measure real-time gas-phase air pollutants such as nitric oxide (NO), nitrogen dioxide (NO_2), carbon dioxide (CO), carbon dioxide (CO_2) and ozone (O_3) have been developed, but proper calibration still poses a challenge (Cao and Thompson, 2016; Mead et al., 2013). For example, Piedrahita et al. (2014) developed wearable air quality monitors (M-Pods) from primarily metal oxide semiconductor sensors. They demonstrated an ability to quantify ambient concentrations of CO, NO_2, CO_2, and O_3, and found that field calibrations, given a wider range of environmental conditions, performed better than laboratory calibrations.

On a larger scale, environmental compliance and policymaking require an understanding of the air pollutant sources and their transport processes, and long-term high-density stationary monitoring networks are needed to ~~fulfill~~fulfil this purpose. In 2010, Mead et al., (2013) deployed 46 sensor nodes in the Cambridge (UK) area for 2.5 months to measure NO, NO_2 and CO. This study demonstrated the feasibility of using low-cost sensors to obtain environmental data at high spatiotemporal resolution. A more recent deployment of two Aerodyne ARISense systems collocated with state air quality stations was described by Cross et al., (2017). ~~This~~ The study reported mixed performance of Alphasense electrochemical NO, CO, NO_2 and O_x (r^2=0.88, 0.84, 0.69, and 0.39) sensors at a 5 min temporal resolution. Numerous state, federal, and international programs continue to evaluate emerging sensor technologies (e.g. South Coast Air Quality Sensor Performance Evaluation Center (AQ-SPEC), EPA Air

Sensor Toolbox, and the World Meteorological Organization (WMO)). For example, the WMO provides a review of low-cost sensor first principles and descriptions of sensor drift and cross-sensitivities by measurement type, including information on many of the sensors used in this study (Lewis et al., 2018). While low-cost sensors have great potential to provide air quality data at higher spatiotemporal resolution and complement existing monitoring sites, multiple studies have reported measurement biases caused by sensor drift due to environmental variables and aging (Borrego et al., 2016; Cross et al., 2017; Lewis et al., 2016; Mead et al., 2013; Zimmerman et al., 2018). Hence, careful sensor characterization, calibration and data processing are important to ensure measurement accuracy.

~~In this study~~In this study~~,~~ we design and evaluate custom stationary and portable multipollutant monitors as part of the SEARCH (Solutions for Energy, AiR, Climate and Health) Center at Yale-Johns Hopkins, which will deploy the multipollutant monitors in a long-term, city-wide network in Baltimore, MD, while also enabling applications in other studies (e.g. ~~(~~Schilling et al., 2020)~~Schilling et al. 2020)~~. ~~-~~Specifically we: (a) describe the physical hardware design, sensors employed, and relevant testing with a focus on overcoming historical limitations; (b) describe and demonstrate the first online calibration system for low-cost monitors; (c) present laboratory tests and field measurements with our monitors to demonstrate real-world performance; (d) compare the performance of the multipollutant monitor to other low-cost monitor deployments; and (e) provide best practices for monitor design to enable future research.

2. Materials & Methods

2.1 Instrument Design

2.1.1 Incorporated Sensors

A suite of sensors is built into the SEARCH multipollutant stationary monitors to measure the concentration of CO, NO_2, NO, CO_2, O_3, methane (CH_4), size-resolved particulate matter (PM), and, when applicable, sulfur dioxide (SO_2). It also collects relative humidity (RH) and temperature (T) data to correct for RH/T influences on sensor response during field deployment with changing environmental conditions. Here the term "monitor" or "multipollutant monitor" is used to describe the collection of sensors and other components (e.g. flow channels, valves, online calibration system) used while the term "sensor" is used to describe the standalone sensing components. Manufacturers and part numbers for the selected sensors are listed in Table 1. Due to size limitations, either a NO or SO_2 sensor is included in the multipollutant monitor based on the application. The monitors evaluated in this study contain NO sensors to better characterize urban NO_x (NO and NO_2) pollution. Monitors with SO_2 sensors will be applied specifically in targeted emissions studies or future locations with higher SO_2 concentrations. The CH_4 and CO_2 sensors are integrated to evaluate greenhouse gas emissions. The portable monitor integrates sensors for CO, CO_2, NO_2, O_3, and PM to evaluate personal exposure in a space-efficient package.

Measurements of CO, NO_2, NO, ~~O_x~~ and SO_2 are made using the 4-electrode electrochemical ppb-level A4 series sensors from Alphasense (http://www.alphasense.com). Different models of electrochemical sensors manufactured by Alphasense have been tested in previous studies (e.g. Hagan et al. (2018), Mead et al. (2013), Zimmerman et al. (2018)) and demonstrate promise for ambient measurements with careful calibration and system design. ~~For the portable monitor's O_x, w~~We used the updated ~~B431~~ A431 model to measure O_x with the portable monitor. The 4-electrode configurations were chosen over the 3-electrode sensors because the extra auxiliary electrode (AE), which has the same functionality as the working electrode (WE) but is not exposed to the analyte, provides a background electrode response. When coupled together with the WE, this reduces the influences of RH/T on sensor signals. Two common concerns for electrochemical and metal oxide sensors are sensor drift over time and cross sensitivity to other pollutants. Electrochemical sensor drift due to sensor aging causes the change of calibration curve intercepts and many studies have shown drift needs to be corrected for deployments over the course of several months (Cross et al., 2017; Hagan et al., 2018). ~~C~~Changes to sensor output by pollutants other than the target analyte are considered cross sensitivities.

~~(~~Pang et al.~~,~~ ~~(~~2018) evaluated pollutant cross sensitivities for the Alphasense (B series) O_3, SO_2, CO, NO, and NO_2 electrochemical sensors and found that while changes in RH were ultimately more important, cross sensitivities at ambient concentrations could contribute to 1-10% of the target pollutant response if uncorrected. For example, they found that the CO electrochemical sensor had a small positive increase in WE voltage with exposure to O_3 and NO_2 while exposure to CO_2 and SO_2 decreased WE voltage.

The Alphasense NDIR sensor measures CO_2, having an estimated limit of detection (LOD) of 1 ppm (Hodgkinson et al., 2013). The NDIR sensor has a broadband light source, and two bandpass filters centered at 4.26 µm and 3.95 µm. The 4.26 µm filter coincides with the CO_2 absorption band centered at 4.2 µm. The 3.95 µm light is not absorbed by CO_2 and works as a reference to account for potential drift in light intensity caused by lamp aging and power supply change. The CO_2 sensor has similar dimensions as the A4 electrochemical sensors.

CH_4 measurements are made using the Figaro TGS2600 gas sensor. Field evaluations of this sensor were performed by Eugster and Kling (2012) in Alaska. More recently, van den Bossche et al. (2017) conducted a systematic laboratory evaluation of a similar Figaro model. Both groups reported measurement agreement between the sensor and a reference technique after correcting for RH and temperature interferences. The Figaro TGS2600 is also sensitive to analytes such as CO, hydrogen (H_2), and volatile organic compounds (VOCs), such as ethanol and isobutane (manufacturer's specification). The cross sensitivity from CO can be corrected in the multipollutant monitor by using the onboard CO sensor. We remove the VOC interference by adding a layer of activated charcoal-impregnated cloth on top of the sensor to filter VOCs. The implementation and performance of this setup is detailed in Sect. 2.1.3.

Formatted: Subscript
Formatted: Subscript
Formatted: Subscript
Formatted: Subscript
Formatted: Subscript
Formatted: Subscript
Formatted: Subscript

For the stationary multipollutant monitor, the MiCS-2614 sensor measures O_3 due to its proven past performance, low cost, and small size (5 mm x 7 mm x 1.55 mm). This sensor was built into a portable ozone monitor by Cao and Thompson (2016) where they found it agreed with 2B Technologies' ozone monitor in the range of 20 ppb to 100 ppb, with over-measurement under 20 ppb and under-measurement above 100 ppb. Note: at the time of this publication, this sensor is not being manufactured.

PM is measured with a miniature PM sensor PMS A003 produced by Plantower (http://www.plantower.com). The sensor has an internal laser and uses scattered light to count particles and differentiate particle size. The device reports mass concentrations in PM_1, $PM_{2.5}$, and PM_{10} with precision of 1 $\mu g/m^3$, as well as particle number concentrations for particle sizes bins: 0.3 µm, 0.5 µm, 1 µm, 2.5 µm, 5 µm, and 10 µm. Levy-Zamora et al. (2019) demonstrated the ability of the sensor to perform under laboratory and ambient settings. With environmental correction factors, the sensor had an overall accuracy of 93% and an overall precision error of 10%. In a Baltimore co-location study, (Datta et al., (2020) utilize the SEARCH multipollutant monitor with Plantower PMS A003 sensors to develop a multiple linear regression calibration with a one day average root mean square error of 2 $\mu g/m^3$. In addition to concerns about environmental factors, it has been shown that the chemical composition of aerosols influences the performance of the Plantower sensor (Levy-Zamora et al., 2019).

2.1.2 Electrical System

The electronics for the multipollutant monitor are designed to have modularized functions on each individual circuit board. Each sensor has its designated analog circuitry to supply power, amplify signals, and filter noise. The analog signals are fed to analog-to-digital converters (ADC) on the daughter boards to minimize noise pick-up in the wiring or other circuitry.

The Alphasense electrochemical sensors are powered with potentiostatic circuitries with zero bias for the CO, NO_2, and SO_2 sensors, and a 200 mV bias for the NO sensor. Special care was taken to match the input impedance for the NO potentiostatic circuit to minimize noise. The circuit amplification is designed to output an analog signal of approximately 1 volt per 100 ppb NO, SO_2, NO_2, and 10 ppm CO. The onboard ADC sequentially converts the amplified and filtered signals generated by the AE and the WE. The AE voltage is recorded as the background signal, and the differential signal between WE and AE voltages is used as the sensor signal for calibration and measurement purposes.

The CO_2 sensor is driven with a 2 Hz 5V 50% duty cycle waveform clocked by a MEMS (Micro-Electro-Mechanical Systems) oscillator. The outputs of the CO_2 sensor are two DC-biased sinusoidal waves from the reference and active channels, and subsequent circuitries are implemented to remove the DC offset and amplify the signals. Two peak detection circuits are applied to sample and hold the peak heights of the two amplified sinusoidal waves to be read sequentially by the ADC. This design uses significantly less processing resources, in comparison with continuous sampling and peak detection through software.

The CH_4 and O_3 circuitries are placed on one circuit board to conserve space and accommodate mechanical requirements (Sect. 2.1.3). These two sensors function by changing their resistances when exposed to their corresponding analytes. Hence, voltage dividers with low temperature coefficient load resistors were applied, and the sensor resistances can be derived by sampling the voltages across the load resistors through ADCs.

The humidity/temperature (RH/T) sensor is placed on a separate small circuit board and towards the front of the inlet to minimize the influence of heat generated by the voltage drop across circuit board traces in the presence of other components. The PM sensor is equipped with a circuit board to convert from its 1 mm pitch connection to a more convenient 2.54 mm pitch connection to facilitate assembly. The RH/T sensor and the PM sensor both output digital signals, and the signals are acquired by the microcontroller directly. Daughter boards for the portable multipollutant monitor are combined or miniaturized versions of the stationary design in order to reduce the amount of wiring and required space.

A central control board generates sensor input voltages, powers components on/off (such as solenoid valves to perform calibration and background measurement), powers a piezoelectric blower (to circulate ambient air for the gas sensors), and reads, processes, stores and transmits sensor data. The control processes use the Cypress 68-pin PSoC 5lp microcontroller, which interfaces with sensors through digital communication peripherals (I2C and UART). The data acquisition frequencies are set as following: the NO_2, NO, SO_2, and CO sensors are sampled every 160 ms, with AE and WE signals each taking up 80 ms sequentially; the CH_4 and O_3 sensors are sampled every 160 ms, utilizing only one signal channel; the RH/T sensor is sampled every 160 ms for either RH data and temperature data sequentially, making their actual sampling period 320 ms; the CO_2 sensor is sampled with 2 Hz frequency in accordance with the input drive frequency for both the active and reference channels; and the PM sensor is sampled every 640 ms, to accommodate its low data output rate relative to the other components. See Table S1 for more information regarding the electronic system.

2.1.3 Mechanical Design

The sampling manifold is designed to isolate the sensing areas of the gas sensors in a small active flow area separated from the rest of the device components (Fig. 1, S3). The manifold is 3D-printed with WaterShed XC11222 resin through stereolithography (SLA), which prints materials with a dense, gas-tight finish. Other 3D printing materials such as acrylonitrile butadiene styrene (ABS) and polylactic acid (PLA) were also tested. These materials are often printed with the fused deposition modeling (FDM) method, creating porous parts that need surface treatment of acetone to be gas-tight. To minimize the potential shape deformation resulting from post-printing treatment, we use the SLA method to print the manifold and other 3D printed parts of the device. O-ring grooves are incorporated in the manifold to secure and provide an air-tight seal for the sensors. To minimize potential ozone loss, the ozone sensor is placed closest to the manifold inlet. In our testing with a 2B-Tech reference ozone monitor, the ozone loss rate is 4–12% for XC11122 resin, versus 7–22% for ABS. To further reduce losses of reactive analyte, a PTFE liner is inserted into the inlet of the XC11122 manifold to reduce contact between the sampling air and the

manifold material. The outlet of the manifold is connected to the piezoelectric blower that sampled at an average flow rate of 0.6 standard liters per minute (SLPM). To optimize monitor response time, the pollutant exchange rate in the manifold is maximized with high flow rates and a small internal volume of ~9 ml, producing an estimated 1 s residence time in the manifold. The ambient air entering the manifold is first pulled through a filter holder with a 2 µm thick, 47 mm diameter Teflon filter to keep the inside of the manifold clean of particles and collect filter samples for offline analysis.

The CH_4 sensor inside the manifold is covered by a layer of activated carbon-impregnated cloth (Zorflex® Double Weave), which is secured by a 3D-printed PLA cylindrical shell. It is then wrapped in Teflon tape in order reduce pollutant interactions with PLA inside of the manifold. This ~~charcoal~~ activated carbon cloth layer is effective in filtering out VOC interference for the sensor. For instance, when covered by the ~~charcoal~~ activated carbon cloth, the CH_4 sensor did not respond to ethanol concentrations as high as 2%. Even after continuous exposure to outdoor VOC for 3 months, with the ~~charcoal~~ activated carbon cloth cover, the CH_4 sensor did not respond to ethanol vapor when an open vial was placed near it. For comparison, when the CH_4 sensor with the used ~~charcoal~~ activated carbon cloth was placed directly above an open vial of ethanol, sensor resistance dropped by approximately 5 kΩ, equivalent to 0.3 ppm methane. While such highly concentrated ethanol vapors are less common in the ambient environment, the activated carbon filter is also likely effective for other VOCs at lower concentrations. Here, ethanol is specifically tested as the challenge compound because the sensor is known to be highly responsive to ethanol and activated carbon is a known, effective hydrocarbon filter for a wide range of VOCs. All calibrations used for in field concentrations include the use of the filter.

Inlet and outlet enclosures are designed for the PM sensor to direct air flow (Fig.1). Specifically, the inlet enclosure contained an SLA 3D-printed Watershed XC11122 holder to support the sensor and an aluminum inlet, through which sample air flows into the sensor inlet. Aluminum was chosen over 3D-printed plastic material as the inlet duct and grounded to the motherboard to avoid electrostatic particle losses due to static charges on a non-metallic surface. The front of the aluminum duct is covered with an aluminum disk placed 30 mm above it, between which a 32 x 32 mesh stainless steel wire cloth is installed to block insects and large dust particles. Ambient air flows through the screen and enters the aluminum channel to reach the sensor inlet. The aluminum disk is placed above the inlet to block light, which was shown to interfere with normal operation and cause the sensor to output PM mass concentrations above 3000 µg/m^3. To reduce the intrusion of light and water, the device is installed with both the gas and particle inlets pointed downwards.

The portable monitor makes all measurements immediately adjacent to the breathing zone with all sensors contained in a small custom shoulder-mountable housing that is 3-D printed and easily attachable to a bag, backpack, purse, or other strap (Fig. 1c–d). A small auxiliary enclosure (23 cm x 12 cm x 6.5 cm; 1 kg including battery) is required to house the re-chargeable battery and main circuit board. The design of the gas sensor manifold is similar to that of the stationary monitor with a piezoelectric blower promoting fast air exchange rates in a minimal volume manifold with PM removed at the inlet via a 23 mm PFTE filter in a PTFE housing. PM is measured via a separate minimal inlet with a light shield.

2.1.4 Online Calibration and Zero System

All monitors undergo multi-point calibrations under variable, realistic RH/T conditions in an environmental chamber prior to field installation. To improve data quality during field deployment and to better track and correct for sensor drift, the stationary monitor includes a laboratory tested span calibration and zero system. These systems are not incorporated into the portable model to conserve space and minimize weight. However, portable monitors will be periodically calibrated in the environmental chamber over the course of the SEARCH project. These features are aimed for helping with long term deployment of the multipollutant monitors. Due to the shorter deployment schedule for this study, we focus only on the calibration and zero system efficacy in laboratory and selected field deployments for proof of concept.

The calibration process has either two or three calibration functions depending on the configuration, with the ability to change the temporal frequency at which each occurs. Each stationary monitor has zeroing functions for both the PM sensor and the gas sensor suite while half of the monitors for the SEARCH deployment also have a gas span calibration function using a miniaturized standard cylinder (dependent upon cylinder composition). In the SEARCH project, the PM and gas zeroing functions are scheduled to occur twice a week and the gas span calibration once a week. Depending on the inclusion of the standard gas cylinder, two or three 3-way solenoid valves are placed in the system to direct flows and alternate normal ambient sampling with PM zero, gas zero, and gas span calibration functions (flow diagram shown in Fig. S4).

For the PM zero, the exhaust from the piezoelectric blower of the gas system, in which particles have been filtered out by a Teflon filter, is directed to the aluminum inlet of the PM sensor. This results in an overflow to the PM inlet due to the higher flow rate of the gas system relative to the particle system, producing a mass concentration of zero.

Zero concentrations for the gas sensors are obtained using either a filtering "zero trap" or via their absence from the calibration cylinder, which is primarily nitrogen and specifically useful for compounds that do not have room-temperature filtration options available for the zero trap. A series of scrubbing materials are used to remove select gas-phase analytes: soda lime for CO_2 and activated carbon and stainless-steel wool for O_3. To obtain the zero-concentration signals with the zero trap, the exhaust of the piezoelectric blower is passed through the packed materials directed to the gas sensors through a side port on the manifold near the inlet. The flow rate through the packed tube is 50 standard cubic centimeters per minute (sccm). With the 9 ml internal volume, the air inside the manifold is re-circulated and passed through the packed tube 16 times in 3 min to ensure complete analyte removal. At the time of writing, we were unable to find materials to effectively remove CH_4, CO, NO_2, and NO at ambient temperatures. Therefore, their zero-concentration signals are determined in the laboratory with zero air prior to field deployment and are checked routinely with the balance of zero air in the calibration cylinder (with the exception of CO and CH_4, which are calibrated via the CO present in the cylinder).

The standard gas delivery system is designed to overflow the manifold with known concentrations of gas standard from a miniature stainless steel gas cylinder (2'' OD x 5.5", Swagelok) that is filled with 5 ppm CO and 2000 ppm CO_2 to 1500 psig

in a balance of nitrogen from a primary authentic cylinder (Airgas). This approach produces a single calibration span value similar to that produced during lab calibration. Prior to installation, the pressure regulator (Tescom) is adjusted, in combination with a 0.006”–0.007” ID PEEK constriction (1/16” OD), to deliver >30 sccm of standard gas flow into the manifold through the exhaust port of the piezoelectric blower with the blower off. Delivery at or above that flowrate is used to ensure constant overflow conditions regardless of cylinder pressure. The components used for the gas delivery system were selected to withstand the pressures of the cylinder and environmental temperatures encountered in the enclosure. Due to concerns over long term chemical stability of certain reactive gases (e.g. NO), only CO and CO_2 are included in the cylinder. The concentrations of the standard gases in the cylinder are also designed to avoid acute exposure concerns. Future work must consider these safety aspects and, given the use of high-pressure gases, should consult with environmental health and safety representatives about any related aspects.

A water permeation setup is included in the standard gas delivery line to maintain a minimum humidity inside the manifold during calibration and prevent unrealistically dry conditions that skew electrochemical sensor response. The water permeation device includes a 3/8” diameter PTFE membrane (0.001” thick, McMaster-Carr) installed in a stainless steel tee (Swagelok) where the membrane separates the standard gas flow from a reservoir of deionized water. The PTFE membrane restricts direct water flow but allows for sufficient permeation of H_2O molecules to raise the humidity of the dry standard gas to a level (>40% in this study) that allows for acceptable calibration conditions. Furthermore, with field operation, RH conditions during calibration can be routinely monitored using the RH/T sensor reporting via the data network. By varying the time of day during which the online calibration occurs, a wide range of realistic RH/T values can be used for assessing sensor drift and to adjust calibration curves.

2.1.5 Cellular Communications and Data Storage

All raw sensor data is written to a local SD card at sub-second frequency. Every 10 s the data is averaged and transmitted to a database hosted on a cloud server through an onboard 4G Telit LE910C1-NS cellular module. To achieve fast and continuous sensor data collection while maintaining simultaneous cellular data transmission, a task preemptive scheduler implemented within the microcontroller firmware tracks the status of the sensors and cellular module and executes core processes (e.g. read, write, send, and receive) at pre-set time intervals. This ensures that all sensor measurements are prioritized over other operating system tasks.

The data streams stored on the SD card and the cloud server include differential, working, and/or auxiliary channels for electrochemical and NDIR sensors, resistances for metal oxide sensors, size-resolved PM mass and number concentration, power supply voltage, and diagnostic information for calibration processes. The InfluxDB time-series database (www.influxdata.com) is used to store, receive and serve sensor data from field-deployed monitors. To maximize data availability, the database is hosted on an Amazon Web Services Elastic Compute Cloud (AWS EC2) instance

(aws.amazon.com). The open-source data visualization platform Grafana (grafana.com) allows users and stakeholders to see real-time field-deployed monitor data remotely through a web browser (see Fig. S5 for screenshots of these data platforms).

2.2 Instrument Evaluation

Our multipollutant monitor undergoes two phases of evaluation in this study: laboratory chamber experiments and ambient co-location with reference instruments. The laboratory experiments provide an isolated environment for characterizing sensor performance and establishing signal-response-to-concentration calibration curves. Outdoor ambient co-location experiments with reference instrumentation test the performance of the monitors over extended periods of time under a variety of real environmental conditions.

For laboratory calibration experiments at Johns Hopkins University, multipollutant monitors are placed inside a custom-built steel chamber (0.71 m x 1.35 m x 0.89 m). Environmental conditions range from 5–85% humidity (most occurring around 30–50%) and 20–40°C. Each gas pollutant is introduced into the chamber through filtered air inlets and diluted to a variety of concentrations above and below typical urban ambient levels using zero air (see Table 2). PM_1, $PM_{2.5}$, and PM_{10} are evaluated using the methodology presented in Levy-Zamora et al. (2019). Online calibration system tests and other sensor response tests at Yale University involve supplying authentic gas standards (Airgas) to the multipollutant monitor inlet or a similar sensor housing. See the SI for linear calibration data (Fig. S6–7) examples and information on how concentration values are calculated for electrochemical sensors.

Field evaluation took place at 3 different locations, dependent on the availability of reference instruments for inter-comparison. They included near an arterial roadway on Yale's campus in New Haven, CT (Wall St.; 3/26/2018–4/7/2018); Baltimore, MD at the State of Maryland Department of the Environment Oldtown site (Oldtown Fire Station, 1100 Hillen St.; 5/18/2017–6/7/2017, 11/2017–12/2017, and 6/14/2018–7/12/2018); as well as in New York, NY (6/23/2018) and Baltimore, MD (3/2/2019) for separate tests of the portable monitor.

The temporal resolution of the comparison between the multipollutant monitor and reference instrumentation is primarily limited by the reference instrument. For NO_2, $PM_{2.5}$, and CO_2 evaluations made at the Oldtown site in MD, the lowest temporal resolution of the reference is 1 hr. For the New Haven, CT field evaluations we use an on-site 2B-Tech (model 202) for O_3 and Thermo Scientific Model 48i for CO and are able to show comparisons at finer time resolution; 1 min for O_3 and 10 min for CO. For comparison to the other sensors and literature, O_3 and CO are also reanalyzed at a 1 h average. In New Haven, 1 h NO reference data is used from the Connecticut Department of Energy and Environmental Protection (DEEP) Criscuolo Park site.

Common metrics for evaluating the performance of sensor configurations include linear regression parameters between RH/T corrected sensor data and reference instrument data such as the coefficient of correlation (r), coefficient of determination (r^2),

slope (m), and intercept (b). Ideal sensor performance would show strong correlation (r=1 or -1, r^2=1) as well as minimal over- or-under estimation of the true concentration (m=1, b=0). Statistical error tests such as the mean bias error (MBE), mean absolute error (MAE), and root mean square error (RMSE) are also commonly used. The MBE represents the tendency for the sensor to over- or under-estimate the reference, although positive and negative errors can cancel each other out. To get around that limitation, the MAE is similar to the MBE but looks only at the average absolute difference between the sensors. Finally, the RMSE represents how narrow the error distribution is by penalizing large measurements errors. All tests are reported in concentration units which allows for physical interpretation of sensor performance. They are calculated as following:

$$MBE = \frac{1}{n}\sum_{i=1}^{n}\left(C_i^{MPM} - C_i^{ref}\right), \quad (1)$$

$$MAE = \frac{1}{n}\sum_{i=1}^{n}\left|C_i^{MPM} - C_i^{ref}\right|, \quad (2)$$

$$RMSE = \sqrt{\frac{1}{n}\sum_{i=1}^{n}\left(C_i^{MPM} - C_i^{ref}\right)^2}, \quad (3)$$

where n is the total number of co-location data points, C^{MPM} is the concentration value of the multipollutant monitor, and C^{ref} is the concentration value of the reference monitor.

3 Results and Discussion

3.1 Stationary Monitor Field Results

3.1.1 Particulate Matter (PM2.5): Comparison of the Plantower PM sensor at the Oldtown site (Baltimore, MD) shows strong correlation (r=0.91, m=1.0) for $PM_{2.5}$ with a 1 h averaging window over the span of 4 weeks. Figure 2a shows a clear overestimate in raw $PM_{2.5}$ by the multipollutant monitor ~~Plantower sensor~~ at higher concentrations, also as reported in Levy-Zamora et al. (2019) for the Plantower sensor, where we derive a ~~laboratory~~ RH/T-correction equation to reduce bias and error (in this study: MBE=+0.9 µg/m^3, RMSE=4.3 µg/m^3). At a separate New Haven, CT deployment, our $PM_{2.5}$ measurements are well-correlated (r=0.94–0.98, m=1.01–1.33) between five different multipollutant monitors at a 10 min resolution (Fig. 2b). See Fig. S8 for the time series data from Fig. 2b.

3.1.2 Nitrogen Dioxide: The NO_2 sensor exhibited strong correlation (r=0.88, m=0.93) at the Oldtown site at hourly resolution. The monitor tracked with the reference well during both clean periods and periods of pollution maxima (MBE=+0.8 ppb, RMSE=5.3 ppb), with concentrations ranging from near zero to over 50 ppb during the deployment (Fig. 3a). Correlation values between the raw multipollutant monitor data and the reference are significantly improved using a RH/T correction (Fig. 3b; see SI for RH/T-correction procedures). In addition, 35% of data points fall within 10% of the reference instrument and 70% fall within 30% (Fig. 3c). The NO_2 sensor is known to be cross sensitive to O_3, but the NO_2 sensors are manufacturer-equipped with an O_3 filter rated to withstand 500 hours at 2 ppm (or longer at lower concentrations). While the NO_2 sensor did

not exhibit cross sensitivity during the Oldtown deployment due to low ozone concentrations, future deployments should take the rating of the ozone filter into consideration and routinely monitor for biases due to ozone.

3.1.3 Carbon Monoxide: The CO sensor demonstrated strong correlation (r=0.92, m=1.2) in a week-long deployment in New Haven, CT at 10 min resolution. Figure 4a shows good tracking of pollution events and background shifts where concentrations exceeded 400 ppb but a noticeable underreporting relative to the reference during these relatively clean periods (<200 ppb). These deviations coincided with elevated temperatures inside the monitor (>15°C) which is consistent with the zero temperature dependence listed by the manufacturer (Alphasense CO-A4 Data Sheet). To correct some of this offset, two sets of temperature corrections were used: a linear fit for all readings above 18°C and a linear fit for all readings below 18°C. Logarithmic and quadratic fits were tested for the high temperature relationship, but the best fit was linear. See Fig. S9 for the low and high temperature data points. Figure 4b shows that even with the correction factors, the overall trend and error (MBE=+5 ppb, RMSE=59 ppb) remain similar to the raw data. After these corrections 43% of data points were within 10% of the reference and 88% were within 30% at a 10 min resolution (Fig. 4c).

3.1.4 Carbon Dioxide: CO_2 showed moderate correlation (r=0.66, m=0.59) with the NIST North-East Corridor Project's NEB tower site over a three-week deployment at a 1 h resolution. While not a direct co-location (2.7 km apart), the NEB site is used as a reference to examine city-wide CO_2 levels and trends while acknowledging that spatial differences from local sources may limit the inter-comparison due to vertical or horizontal variance. Figure 5a shows the monitor trends well with the reference after temperature-correction, although the monitor occasionally exceeds the reference concentration by 10-20 ppm (MBE=+3.4 ppm, RMSE=11 ppm). This is consistent with the reported accuracy of ~15 ppm shown in the manufacturer data sheet at 400 ppm in laboratory testing (Alphasense IRC-A1 Data Sheet). Possible lags in regional pollution episodes can be observed in the time series data (e.g. 6/30, 7/1, 7/7) leading to a lower correlation value than other presented pollutants. Despite this, 70% of readings were within 2.5% of the reference instrument (~10 ppm) and 98% were within 7.5% (~30 ppm).

3.1.5 Ozone: The O_3 sensor exhibited strong correlation (r=0.97, m=0.99) at a high temporal resolution of 1 min in New Haven, CT. The raw sensor resistance followed the ozone concentration measured by the 2B monitor with an exponential relationship (Fig. 6b). With this fitted exponential curve, the ozone concentration from sensor measurement was derived, and compared to the 2B monitor results to evaluate the sensor's performance and dependency on environmental factors (MBE=-0.2 ppb, RMSE=3.3 ppb). We found that at low ozone concentrations (<10 ppb), there is considerable measurement discrepancy between the two devices (Fig. 6c-d). This is consistent with the sensor manufacturer's 10–1000 ppb rating for the device's measurement range (Table 1). For ozone concentrations higher than 10 ppb, 67% of the data points agree within 10%, and 99% within 30% of the reference (Fig. 6e). It is worth noting that the sensor output was not significantly affected by changes in RH during the study, despite large variation in these environmental conditions (Fig. 6d). The temperature effect is more significant with the concentration ratio for our monitor to the reference (for data >10 ppb), following the relationship

0.85 + 0.70 exp(-0.11T). Still, the sensor's temperature biases are minor here as Fig. 6e presents non-temperature-corrected results.

3.1.6 Nitric Oxide: Without an immediately co-located reference NO monitor, we compared the NO sensor performance against the near-road DEEP Criscuolo Park site (1.6 km away from sampling location in downtown New Haven). The sensor had higher error terms than other low ppb-level sensors (MBE=+1.6, RMSE=16 ppb) likely due to the distance difference and deviations due to local dynamics, but still showed good agreement (Fig. 7) and reasonable correlation (r=0.74, m=0.86; Fig. S11) at a 1 h resolution. We also leverage O_3 and CO measurements during the same sampling window to understand NO concentrations as NO readily reacts with O_3 and is often co-emitted with CO during combustion. The two-week campaign shows the effect of high NO concentrations on O_3 abundances due to the reaction NO + O_3, and CO enhancements coincide with elevated NO concentration levels (Fig. 7). NO concentrations at 1 h resolution during the New Haven deployment range from 0 to 160 ppb with three major concentration enhancements. Each buildup occurred overnight and dissipated around mid-morning, potentially owing to periods of decreased ventilation and the accumulation of NO from nighttime traffic emissions in the nocturnal boundary layer without any photochemistry. A 1 h time lag relative to the reference site is observed on some NO spikes which is also observed in the CO data, and is likely due to differences in sampling location. During the three periods when NO concentrations exceeded 100 ppb for an extended period of time, O_3 concentrations decreased to ~0 ppb and CO concentrations exceeded 600 ppb. It is worth noting that the NO sensor used does not have significant cross-response to O_3 or CO (Alphasense NO-A4 Data Sheet).

3.1.7 Others: Other pollutants not discussed in detail here include CH_4 and SO_2. The Figaro TGS2600 methane sensor demonstrated high linearity in signal response in the laboratory (Fig. S7) and effective VOC filtration, but a reference monitor was not available and future testing is planned. While the multipollutant monitors field-tested in this paper do not include the SO_2 sensor, and it is not planned for the SEARCH deployment, our laboratory results (Fig. S6) and past work (Hagan et al., 2018) suggest it is suitable for measurements in locations with SO_2 concentrations higher than typical urban levels (>15 ppb).

3.2 Portable Monitor Field Testing

Personal exposure data was collected using our shoulder-mounted portable monitor in Manhattan, New York City (Fig. 8), and Baltimore, MD (Fig. 9). These results are discussed in brief with a focus on $PM_{2.5}$. In New York City, $PM_{2.5}$ concentrations reached a maximum of 210 µg/m^3 at a restaurant where the average was 34 µg/m^3 while inside. Several closely occurring spikes with $PM_{2.5}$ maxima at 30–175 µg/m^3 occurred in an area with food carts on Broadway Ave. between 34th and 57th St., including open flame meat cooking, small power generators, and cigarette smoking. An average concentration of 9 ± 21 µg/m^3 was encountered across the 6 h period that included a mix of indoor and outdoor environments, and a mix of parks and streets. Concentrations while in parks were lower than when walking along streets. The average concentrations across the southern transect of Central Park (5:45 pm) and Madison Square Park (7:30 pm) were 0.5 µg/m^3 and 1.4 µg/m^3, respectively, compared to 3.9 µg/m^3 while on the streets before and after. Coupling the high sampling rate of one measurement per second

with RH/T correction factors, the portable monitor has the ability to capture high-temporal resolution events (i.e., 10–20 s) for $PM_{2.5}$. PM_1 had similar trends, with a $PM_{2.5}/PM_1$ ratio of 1.44 at the restaurant, 1.48 at the parks, and 1.44 for the entire study period. Due to the lack of a robust RH/T correction factor for PM_1, we report only the ratio for $PM_{2.5}/PM_1$ in the raw data.

A day-long deployment in Baltimore shows $PM_{2.5}$ concentrations vary widely across locations and transportation modes (Fig. 9) and can be mapped within a city via GPS. Elevated levels of 35 µg/m^3 occurred in the morning at a restaurant before reaching consistent values of less than 10 µg/m^3 for most of the day. There were occasional concentration spikes, such as walking through a commercial store (see purple symbols at 11:00am) where measurements rapidly rose from ~0 to 30 µg/m^3. In the afternoon, concentrations spiked to above 110 µg/m^3 while driving during rush hour with the windows closed. GPS functionality was maintained throughout the study and accurately depicted the path of the participant, yet some path information in Fig. 9 is not depicted during vehicle transport due to averaging to 1 min intervals.

3.3 Sensor Response Time

A key performance characteristic of any field-deployed analytical instrument is its response time to changes in pollutant concentrations, especially in dynamic urban environments where concentrations change rapidly with source proximity or microenvironments. This response time is a function of air exchange rates within the sampling system and the individual sensor response times, which are inherently limited in some sensors involving electrochemical processes. A useful metric to examine this is the e-folding time (i.e. a decrease to a signal of 1-1/e or ~63%) of sensor signals due to abrupt changes in pollutant concentration. A long e-folding time indicates a sluggish sensor, while a short e-folding time indicates a responsive sensor that can respond to a dynamic environment and distinguish changes at higher-temporal resolution. To characterize the sample delivery systems, Fig. 10 shows the response of several sensors in the multipollutant monitor and their e-folding times. $PM_{2.5}$ has the shortest e-folding time of roughly 10 s (PM_1 and PM_{10} are similar) due to its optical sensing technique (in a separate sampling inlet). CO and CO_2 have similar e-folding times of 20 s, demonstrating an ability to capture changes at under 1 min resolution (see Fig. S10 for analysis of 20 s PM_1 and CO roadside plumes). NO and NO_2 take longer to respond, 50 and 65 s respectively, but are still capable of capturing urban dynamics at a 5–10 min resolution.

3.4 Online Calibration Processes

3.4.1 Standard Gas Cylinder Delivery: A laboratory test of the gas cylinder delivery system is shown in Fig. 11a delivering known concentrations of CO and CO_2 in a balance of nitrogen for a span check as well as zero concentration signals for other sensors (e.g. NO_2, NO). With the small internal volume of the manifold flushed by 30 sccm of standard gas, it quickly reaches stabilized signals within the 3 min calibration periods, consistent with expectations based on Fig.10. Five repeated runs at a delivery pressure of 35 psig (prior to the constriction tubing that substantially reduces pressure to near 1 atm) demonstrated consistent behavior and is representative of initial performance in field tested units. Expected shifts in RH are observed (and

can be used in-field to evaluate RH sensitivity), but the permeation device maintains humidity at relevant conditions despite a completely dry standard gas.

3.4.2 Zero Trap: Figure 11b shows the effective removal of CO_2 using the gas zeroing function, while stable concentrations are observed for non-zeroed gases. Changes in NO concentrations (and less so for NO_2) occur due to the observed changes in RH. During long-term field deployment, RH changes occurring both during the use of the calibration gas cylinder and the zero trap are also useful indicators to check in-field RH-dependent changes in response factors and zero signals, respectively, when occurring under stable concentrations. Similarly, differences in temperature between zeroing periods can be used to check temperature-related variations for sensors with significant temperature response. Figure 11b does not include O_3 data as the levels in the laboratory were too low for sensor response to move off the baseline. Experiments at higher concentrations indicate that stainless steel is an effective scavenger of O_3 (see Fig. S12).

3.4.3 PM Zero: Field testing of the PM zero method was conducted near food cart vendors in New Haven, CT. Ambient concentrations ranged between 3 and 48 µg/m^3 with rapid changes due to moderate wind levels and proximity to active sources. After switching the valves, PM levels were effectively zeroed for two minutes and rose back immediately to higher concentrations and saw large spikes after the zero ended (see Fig. S13). For monitors in very close proximity to highly-concentrated plumes (e.g., >250 µg/m^3), longer zero periods or scheduling during low activity periods may be necessary to fully flush the inlet and avoid/isolate bias from concentrated plumes.

3.5 Comparison with Literature

To contextualize the performance of our monitors, Table~~s~~ 3 (for NO_2, NO, and CO) and 4 (for CO_2, O_3, and $PM_{2.5}$) show~~s~~ a summary of co-location statistical data with several recent literature field deployments. For a more extensive comparison, see Karagulian et al. (2019). The presented performance metrics are specific to the region and conditions they were evaluated in, and differences in sampling locations, environmental conditions, pollutant mixtures, and testing durations should be considered in future applications. For NO_2, our multipollutant monitor had a higher r^2 (0.77) than other studies except for Bigi et al. (2018) (r^2=0.80), with our MAE and RMSE lower by 2.1 and 3 ppb, respectively. The NO sensor shows lower correlation than other studies such as Cross et al. (2017) in terms of r^2 (their r^2 of 0.84 compared to our 0.54) and error terms (their RMSE of 4.52 ppb compared to our 16 ppb), though we are comparing against a reference instrument located 1.6 km away with evident localized dynamics (see Sect. 3.1.6). For CO, the multipollutant monitor performed similarly to other studies using Alphasense electrochemical sensors, such as Zimmerman et al. (2018), where our r^2 and MAE were lower by 0.11 and 3 ppb, respectively. To our knowledge this work is the first low-cost urban air sensor network implementation of the Alphasense IRC-A1 sensor. Zimmerman et al. (2018) measured CO_2 using an SST CO2S-A, but no reference instrument was available for their co-location study. One study that did report CO_2 co-location results was ~~Spinelle et al. (2017) (~~Spinelle et al., 2017~~)~~, which showed higher r^2 (0.51–0.79) but similar slope values after using an artificial neural network for calibration. ~~(~~Shusterman et al.~~,~~ (2016), as a

Formatted: Subscript
Formatted: Subscript
Formatted: Subscript
Formatted: Subscript

part of the BErkeley Atmospheric CO2 Observation Network implement a more expensive, yet still lower cost than reference instrumentation, Vaisala CarboCap GMP343 with extremely high correlation (r^2=0.999) during a 5-day comparison. For O_3, the deployments used for comparison primarily utilized a form of the Alphasense Ox-B4 sensor (in tandem with NO_2 electrochemical sensors). Our MiCS sensor performed well compared to other co-locations in regards to r^2 and m values, with only Zimmerman et al. (2018) (using the ~~the same~~ updated Ox-B431, which ~~we~~ is similar to the A431 which we employ in our portable monitors) reporting similar MBE. Ripoll et al. (2019) used both an Alphasense Ox-B431 and MiCS-2614 sensor and found that both exhibited strong performance, similar to our results. For $PM_{2.5}$, we compare our sensors primarily with selected results from AQ-SPEC testing (i.e. five highest r^2 values) from Feenstra et al. (2019). $PM_{2.5}$ sensors saw a wide range of r^2 values being reported (0.73–0.95) with the highest coming from the PurpleAir PA-II which uses a Plantower sensor and the two next highest being Plantower A003 sensors from this study. To summarize the performance distribution of our pollutant measurements, Fig. S14 compares the values from Tables 3 and 4 to the "best selection region" defined by Karagulian et al. (2019).

Formatted: Superscript

Formatted: English (United States)

3.6 Best Practices

The field of low-cost air quality sensors is rapidly improving, and new generations of monitoring devices should strive to further improve accuracy and precision. Here we present a list of lessons learned, obstacles faced, and recommendations for future design, fabrication, and deployment. Careful consideration of electronic design and sensor selection can eliminate complications later in the process. We make the following recommendations: choose low noise components where applicable to enhance precision and improve detection limits; transform signals from analog to digital near to the sensor to preserve signal; utilize ADCs of sufficiently high resolution for the application to achieve the resolution necessary for the pollutant measurement application; use electronic shielding on sensitive sensing or signal transmission components; monitor power delivery in real time and report back auxiliary and supply signals; and measure RH/T dependent channels where applicable (e.g. auxiliary electrode on Alphasense sensors).

Good design should take into account sensor-to-sensor performance and practice good quality assurance and quality control (QA/QC) of sensors, both prior to installation and for a trial period after installation. For some of the sensors used in the multipollutant monitor, there was more deviation from lot-to-lot than anticipated which requires careful laboratory calibration to correct. To minimize the impact of sensor variability on field measurements, characterize sensors before installation and deployment for supplemental quality control purposes. If possible, compare new sensors against typical response patterns found in the deployment already in order to gauge whether a sensor or circuit board may be malfunctioning early on. With a large network, some amount of automation will be necessary to quickly determine malfunctioning monitors. Also, carefully consider the position within the manifold and implement measures to keep the sensors clean and away from interferences, such as upstream particle filtration for gas-phase sensors or positioning the NDIR CO_2 sensor last to reduce the influence of waste heat, respectively.

Active flow is critical and allows us to achieve high temporal resolution measurements with e-folding times below one minute for most pollutants. In urban settings and for personal exposure studies this provides additional data points to identify rapidly changing emissions and environmental conditions. When deploying the monitors: use a water-tight enclosure with inlets pointed downwards to avoid light and water intrusion; shade them from direct sunlight if possible at a given site to reduce temperature swings that exacerbate temperature-dependent calibration changes; implement mesh to the inlets to prevent insects from entering; and be mindful of point source emissions nearby to reduce undesired bias. Additionally, check for flow balance consistently during construction and then periodically in the field (during deployment or servicing) to (i) confirm high active flow rates, (ii) verify that measurements are not being compromised with air from within the enclosure, and (iii) ensure that on-board calibrations perform properly. Additionally, in order to better assess issues remotely, choice of wireless connectivity should be evaluated. Cell connections are convenient and allow for the monitor to be placed nearly anywhere but can be spotty at times and can be more expensive to operate than a WiFi-based approach. Protocols for remote access into the monitors to address problems and prompt a restart are desirable to minimize wasted travel time to sites.

4 Conclusions

Our multipollutant monitors advance the state of the field by monitoring 9+ gas and size-resolved PM pollutant data streams simultaneously in an optimized fast-response active flow system. The stationary monitor includes a novel on-board calibration system and the portable shoulder-mountable monitor samples in the breathing zone. We implement low-noise electronic design, GPS tracking, and cellular communications to communicate ambient and calibration data in real-time—all to enable more accurate and precise cost-effective monitor networks for stationary or mobile platforms. The calibration system is flexible and can be adjusted for a variety of analytes of interest via tuning of the calibration gas or zero trap. Additionally, a greater range of RH/T points can be gained by increasing calibration frequency with strategic timing of calibration functions across the day. Still, there is a need for continual long-term evaluation and improvement of laboratory and field calibration procedures, effects from RH/T, and comparisons to reference instrumentation through permanent and temporary co-location. With most pollutants achieving high correlation in urban field evaluations, these systems are ready for large-scale network deployments and smaller scale targeted measurements.

Code/Data Availability

Data will be made available by the authors upon request.

Supporting Information

Figures S1–14 and Table S1 are available in the Supporting Information (PDF), available free of charge online.

Author Contributions

FX, MLZ, BK, KR, KMS, JKG, KK, and DRG conceptualized the multipollutant monitor mechanical design, electronics, and/or online calibration system. CB, FX, MLZ, JKG, SC, MM, and DRG designed and constructed the multipollutant monitors or tested their components. CB, FX, MM, and MLZ performed calibration testing. CB, FX, MLZ, CR, and DRG performed co-location experiments and/or collected data. CB, FX, and MLZ performed data analysis. MB, BW, and BK helped design and develop electronics, cellular communications, data management. KR also provided guidance on the electronic design and best practices. CB, FX, and DRG prepared ~~of~~ the original manuscript. All authors have reviewed the paper.

Formatted: Font color: Text 1

Competing Interests

DRG has externally-funded projects on low-cost air quality monitoring technology (EPA, HKF Technology), where the developed technology has been licensed by Yale to HKF Technology.

Acknowledgements

We thank HKF Technology, the U.S. Environmental Protection Agency, and The Heinz Endowments for funding the research. C.B., D.R.G., K.K., B.K., and M.L.Z. acknowledge support from the Assistance Agreement No. RD835871 awarded by the U.S. Environmental Protection Agency to Yale University. It has not been formally reviewed by EPA. The views expressed in this document are solely those of the authors and do not necessarily reflect those of the Agency. EPA does not endorse any products or commercial services mentioned in this publication. C.B. is supported by the National Science Foundation Graduate Research Fellowship Program under Grant No. DGE1752134. Any opinions, findings, and conclusions or recommendations expressed in this material are those of the author(s) and do not necessarily reflect the views of the National Science Foundation. M.L.Z. was also supported by the National Institute of Environmental Health Sciences of the National Institutes of Health under awards number 1K23ES029985-01 and K99ES029116. The content is solely the responsibility of the authors and does not necessarily represent the official views of the National Institutes of Health. The authors thank the Maryland Department of the Environment Air and Radiation Management Administration for allowing us to colocate our sensors with their instruments. For their assistance, we thank the Yale Center for Engineering Innovation and Design (CEID); Jordan Peccia (Yale); the following Yale undergraduates for their assistance: Kevin Truong, Hannah Nesser, Patrick Wilczynski, Genevieve Fowler, Mieke Scherpbier, Jonathan Chang, Christian White, Marissa Huiling Foo, Reese Roberts, Bohan Lou, Christian Mendez, Tori Hass-Mitchell, Jinny Van Doorn, Pulith Peiris; and Amir Bond and Ethan Weed (Peabody EVOlutions). We thank Alphasense for their help with sensor integration and signal processing.

References

Alphasense Ltd.: IRC-A1 Carbon Dioxide Infrared Sensor Data Sheet, [online] Available from: http://www.alphasense.com/WEB1213/wp-content/uploads/2018/04/IRC-A1.pdf, 2018.

Alphasense Ltd.: CO-A4 Carbon Monoxide Sensor Data Sheet, [online] Available from: http://www.alphasense.com/WEB1213/wp-content/uploads/2019/09/CO-A4.pdf, 2019a.

Alphasense Ltd.: NO-A4 Nitric Oxide Sensor Data Sheet, [online] Available from: http://www.alphasense.com/WEB1213/wp-content/uploads/2019/09/NO-A4.pdf, 2019b.

Bigi, A., Mueller, M., Grange, S. K., Ghermandi, G. and Hueglin, C.: Performance of NO, NO2 low cost sensors and three calibration approaches within a real world application, Atmos. Meas. Tech., 11(6), 3717–3735, doi:10.5194/amt-11-3717-2018, 2018.

Borrego, C., Costa, A. M., Ginja, J., Amorim, M., Coutinho, M., Karatzas, K., Sioumis, T., Katsifarakis, N., Konstantinidis, K., De Vito, S., Esposito, E., Smith, P., André, N., Gérard, P., Francis, L. A., Castell, N., Schneider, P., Viana, M., Minguillón, M. C., Reimringer, W., Otjes, R. P., von Sicard, O., Pohle, R., Elen, B., Suriano, D., Pfister, V., Prato, M., Dipinto, S. and Penza, M.: Assessment of air quality microsensors versus reference methods: The EuNetAir joint exercise, Atmos. Environ., 147(2), 246–263, doi:10.1016/j.atmosenv.2016.09.050, 2016.

van den Bossche, M., Rose, N. T. and De Wekker, S. F. J.: Potential of a low-cost gas sensor for atmospheric methane monitoring, Sensors Actuators, B Chem., 238(2), 501–509, doi:10.1016/j.snb.2016.07.092, 2017.

Brauer, M., Amann, M., Burnett, R. T., Cohen, A., Dentener, F., Ezzati, M., Henderson, S. B., Krzyzanowski, M., Martin, R. V., Van Dingenen, R., Van Donkelaar, A. and Thurston, G. D.: Exposure assessment for estimation of the global burden of disease attributable to outdoor air pollution, Environ. Sci. Technol., 46(2), 652–660, doi:10.1021/es2025752, 2012.

Cao, T. and Thompson, J. E.: Personal monitoring of ozone exposure: A fully portable device for under $150 USD cost, Sensors Actuators, B Chem., 224, 936–943, doi:10.1016/j.snb.2015.10.090, 2016.

Castell, N., Dauge, F. R., Schneider, P., Vogt, M., Lerner, U., Fishbain, B., Broday, D. and Bartonova, A.: Can commercial low-cost sensor platforms contribute to air quality monitoring and exposure estimates?, Environ. Int., 99, 293–302, doi:10.1016/j.envint.2016.12.007, 2017.

Chuang, K. J., Chan, C. C., Su, T. C., Lee, C. Te and Tang, C. S.: The effect of urban air pollution on inflammation, oxidative stress, coagulation, and autonomic dysfunction in young adults, Am. J. Respir. Crit. Care Med., 176(4), 370–376, doi:10.1164/rccm.200611-1627OC, 2007.

Cohen, A. J., Brauer, M., Burnett, R., Anderson, H. R., Frostad, J., Estep, K., Balakrishnan, K., Brunekreef, B., Dandona, L., Dandona, R., Feigin, V., Freedman, G., Hubbell, B., Jobling, A., Kan, H., Knibbs, L., Liu, Y., Martin, R., Morawska, L., Pope, C. A., Shin, H., Straif, K., Shaddick, G., Thomas, M., van Dingenen, R., van Donkelaar, A., Vos, T., Murray, C. J. L. and Forouzanfar, M. H.: Estimates and 25-year trends of the global burden of disease attributable to ambient air pollution: an analysis of data from the Global Burden of Diseases Study 2015, Lancet, 389(10082), 1907–1918, doi:10.1016/S0140-

6736(17)30505-6, 2017.

Cross, E. S., Williams, L. R., Lewis, D. K., Magoon, G. R., Onasch, T. B., Kaminsky, M. L., Worsnop, D. R. and Jayne, J. T.: Use of electrochemical sensors for measurement of air pollution: Correcting interference response and validating measurements, Atmos. Meas. Tech., 10(9), 3575–3588, doi:10.5194/amt-10-3575-2017, 2017.

Datta, A., Saha, A., Zamora, M. L., Buehler, C., Hao, L., Xiong, F., Gentner, D. R. and Koehler, K.: Statistical field calibration of a low-cost PM2.5 monitoring network in Baltimore, Atmos. Environ., 242(March), 117761, doi:10.1016/j.atmosenv.2020.117761, 2020.

Eugster, W. and Kling, G. W.: Performance of a low-cost methane sensor for ambient concentration measurements in preliminary studies, Atmos. Meas. Tech., 5(8), 1925–1934, doi:10.5194/amt-5-1925-2012, 2012.

Feenstra, B., Papapostolou, V., Hasheminassab, S., Zhang, H., Boghossian, B. Der, Cocker, D. and Polidori, A.: Performance evaluation of twelve low-cost PM2.5 sensors at an ambient air monitoring site, Atmos. Environ., 216(August), 116946, doi:10.1016/j.atmosenv.2019.116946, 2019.

Forouzanfar, M. H., Afshin, A., Alexander, L. T., Biryukov, S., Brauer, M., Cercy, K., Charlson, F. J., Cohen, A. J., Dandona, L., Estep, K., Ferrari, A. J., Frostad, J. J., Fullman, N., Godwin, W. W., Griswold, M., Hay, S. I., Kyu, H. H., Larson, H. J., Lim, S. S., Liu, P. Y., Lopez, A. D., Lozano, R., Marczak, L., Mokdad, A. H., Moradi-Lakeh, M., Naghavi, M., Reitsma, M. B., Roth, G. A., Sur, P. J., Vos, T., Wagner, J. A., Wang, H., Zhao, Y., Zhou, M., Barber, R. M., Bell, B., Blore, J. D., Casey, D. C., Coates, M. M., Cooperrider, K., Cornaby, L., Dicker, D., Erskine, H. E., Fleming, T., Foreman, K., Gakidou, E., Haagsma, J. A., Johnson, C. O., Kemmer, L., Ku, T., Leung, J., Masiye, F., Millear, A., Mirarefin, M., Misganaw, A., Mullany, E., Mumford, J. E., Ng, M., Olsen, H., Rao, P., Reinig, N., Roman, Y., Sandar, L., Santomauro, D. F., Slepak, E. L., Sorensen, R. J. D., Thomas, B. A., Vollset, S. E., Whiteford, H. A., Zipkin, B., Murray, C. J. L., Mock, C. N., Anderson, B. O., Futran, N. D., Anderson, H. R., Bhutta, Z. A., Nisar, M. I., Akseer, N., Krueger, H., Gotay, C. C., Kissoon, N., Kopec, J. A., Pourmalek, F., Burnett, R., Abajobir, A. A., Knibbs, L. D., Veerman, J. L., Lalloo, R., Scott, J. G., Alam, N. K. M., Gouda, H. N., Guo, Y., McGrath, J. J., Jeemon, P., Dandona, R., Goenka, S., Kumar, G. A., Gething, P. W., Bisanzio, D., et al.: Global, regional, and national comparative risk assessment of 79 behavioural, environmental and occupational, and metabolic risks or clusters of risks, 1990–2015: a systematic analysis for the Global Burden of Disease Study 2015, Lancet, 388(10053), 1659–1724, doi:10.1016/S0140-6736(16)31679-8, 2016.

Hagan, D. H., Isaacman-Vanwertz, G., Franklin, J. P., Wallace, L. M. M., Kocar, B. D., Heald, C. L. and Kroll, J. H.: Calibration and assessment of electrochemical air quality sensors by co-location with regulatory-grade instruments, Atmos. Meas. Tech., 11(1), 315–328, doi:10.5194/amt-11-315-2018, 2018.

Hodgkinson, J., Smith, R., Ho, W. O., Saffell, J. R. and Tatam, R. P.: Non-dispersive infra-red (NDIR) measurement of carbon dioxide at 4.2 μm in a compact and optically efficient sensor, Sensors Actuators, B Chem., 186, 580–588, doi:10.1016/j.snb.2013.06.006, 2013.

Karagulian, F., Barbiere, M., Kotsev, A., Spinelle, L., Gerboles, M., Lagler, F., Redon, N., Crunaire, S. and Borowiak, A.: Review of the performance of low-cost sensors for air quality monitoring, Atmosphere (Basel)., 10(9),

doi:10.3390/atmos10090506, 2019.

Kheirbek, I., Wheeler, K., Walters, S., Kass, D. and Matte, T.: PM2.5 and ozone health impacts and disparities in New York City: Sensitivity to spatial and temporal resolution, Air Qual. Atmos. Heal., 6(2), 473–486, doi:10.1007/s11869-012-0185-4, 2013.

Kim, J., Shusterman, A. A., Lieschke, K. J., Newman, C. and Cohen, R. C.: The Berkeley Atmospheric CO2 Observation Network: Field calibration and evaluation of low-cost air quality sensors, Atmos. Meas. Tech., 11(4), 1937–1946, doi:10.5194/amt-11-1937-2018, 2018.

Levy-Zamora, M., Xiong, F., Gentner, D., Kerkez, B., Kohrman-Glaser, J. and Koehler, K.: Field and Laboratory Evaluations of the Low-Cost Plantower Particulate Matter Sensor, Environ. Sci. Technol., 53(2), 838–849, doi:10.1021/acs.est.8b05174, 2019.

Lewis, A. C., Lee, J. D., Edwards, P. M., Shaw, M. D., Evans, M. J., Moller, S. J., Smith, K. R., Buckley, J. W., Ellis, M., Gillot, S. R. and White, A.: Evaluating the performance of low cost chemical sensors for air pollution research, Faraday Discuss., 189, 85–103, doi:10.1039/c5fd00201j, 2016.

Lewis, A. C., von Schneidemesser, E. and Peltier, R. E.: Low-cost sensors for the measurement of atmospheric composition: overview of topic and future applications. [online] Available from: http://www.wmo.int/pages/prog/arep/gaw/documents/Draft_low_cost_sensors.pdf, 2018.

Mead, M. I., Popoola, O. A. M., Stewart, G. B., Landshoff, P., Calleja, M., Hayes, M., Baldovi, J. J., McLeod, M. W., Hodgson, T. F., Dicks, J., Lewis, A., Cohen, J., Baron, R., Saffell, J. R. and Jones, R. L.: The use of electrochemical sensors for monitoring urban air quality in low-cost, high-density networks, Atmos. Environ., 70, 186–203, doi:10.1016/j.atmosenv.2012.11.060, 2013.

Pang, X., Shaw, M. D., Gillot, S. and Lewis, A. C.: The impacts of water vapour and co-pollutants on the performance of electrochemical gas sensors used for air quality monitoring, Sensors Actuators, B Chem., 266, 674–684, doi:10.1016/j.snb.2018.03.144, 2018.

Piedrahita, R., Xiang, Y., Masson, N., Ortega, J., Collier, A., Jiang, Y., Li, K., Dick, R. P., Lv, Q., Hannigan, M. and Shang, L.: The next generation of low-cost personal air quality sensors for quantitative exposure monitoring, Atmos. Meas. Tech., 7(10), 3325–3336, doi:10.5194/amt-7-3325-2014, 2014.

Pope, C. A. and Dockery, D. W.: Health effects of fine particulate air pollution: Lines that connect, J. Air Waste Manag. Assoc., 56(6), 709–742, doi:10.1080/10473289.2006.10464485, 2006.

Popoola, O. A. M., Stewart, G. B., Mead, M. I. and Jones, R. L.: Development of a baseline-temperature correction methodology for electrochemical sensors and its implications for long-term stability, Atmos. Environ., 147, 330–343, doi:10.1016/j.atmosenv.2016.10.024, 2016.

Schilling, K., Gentner, D. R., Wilen, L., Medina, A., Buehler, C., Perez-Lorenzo, L. J., Pollitt, K. J. G., Bergemann, R., Bernardo, N., Peccia, J., Wilczynski, V. and Lattanza, L.: An accessible method for screening aerosol filtration identifies poor-performing commercial masks and respirators, J. Expo. Sci. Environ. Epidemiol., doi:10.1038/s41370-020-0258-7, 2020.

Shusterman, A. A., Teige, V. E., Turner, A. J., Newman, C., Kim, J. and Cohen, R. C.: The Berkeley Atmospheric CO2 Observation Network: Initial evaluation, Atmos. Chem. Phys., 16(21), 13449–13463, doi:10.5194/acp-16-13449-2016, 2016.

Spinelle, L., Gerboles, M., Villani, M. G., Aleixandre, M. and Bonavitacola, F.: Field calibration of a cluster of low-cost commercially available sensors for air quality monitoring. Part B: NO, CO and CO2, Sensors Actuators, B Chem., 238, 706–715, doi:10.1016/j.snb.2016.07.036, 2017.

Thorson, J., Collier-Oxandale, A. and Hannigan, M.: Using A Low-Cost Sensor Array and Machine Mixtures and Identify Likely Sources, Sensors, 19, 3723, 2019.

Zimmerman, N., Presto, A. A., Kumar, S. P. N., Gu, J., Hauryliuk, A., Robinson, E. S., Robinson, A. L. and Subramanian, R.: A machine learning calibration model using random forests to improve sensor performance for lower-cost air quality monitoring, Atmos. Meas. Tech., 11(1), 291–313, doi:10.5194/amt-11-291-2018, 2018.

.

Table 1: Technical specifications concerning the pollutant and environmental sensors tested and used~~used~~.

Sensor Target	~~Manufacturer and~~ Part Number	Method	Observed LOD	Usage[c]
CO	Alphasense CO-A4	4-electrode electrochemical	20 ppb	S, P
NO	Alphasense NO-A4	4-electrode electrochemical	3 ppb	S
NO_2	Alphasense NO2-A43F	4-electrode electrochemical	1 ppb	S, P
SO_2	Alphasense SO2-A4	4-electrode electrochemical	15 ppb	-
O_3	Alphasense OX-A431	4-electrode electrochemical	1 ppb	P
CO_2	Alphasense IRC-A1	Infrared, pyroelectric	[a]	S, P
CH_4	Figaro TGS 2600	Metal oxide resistance	[a]	S
O_3	MiCS-2614	Metal oxide resistance	10 ppb	S
PM_1, $PM_{2.5}$, PM_{10}	Plantower A003	Optical particle counter	1 µg/m^3	S, P
RH & T	Sensirion SHT25	-	0-100 %, 0-120 °C[b]	S, P

[a]Below ambient background concentrations. [b]From manufacturer data sheet. [c]Used in the stationary (S) and/or portable (P) version of the multipollutant monitor.

Table 2: Lab calibration procedure and environmental condition ranges for gases. Each non-zero gas concentration is maintained for 90 minutes.

Gas	Concentrations/Ranges
NO	0, 5, 10, 30, 50 ppb
CO	0, 1, 2, 3, 4 ppm
O_3	10, 20, 50, 75, 100 ppb*
NO_2	0, 5, 10, 30, 50 ppb
CH_4	1, 1.5, 2, 2.5 ppm
CO_2	400, 500, 700 ppm
RH	5-85 %
T	20-40 °C

*Denotes that each concentration is repeated

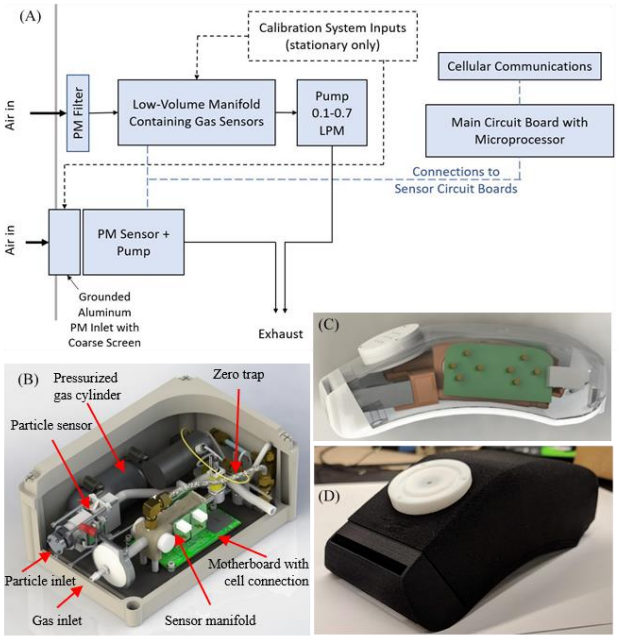

Figure 1: Monitor designs shown as (a) simplified flow and electronics diagram, which is used in the (b) stationary (28 x 18 x 14 cm) and (c-d) portable (15 x 6.5 x 5 cm) versions of the multipollutant monitoring device. Panels b-c are solidworks renderings, and d is a photo. See Fig. S3 for additional photos.

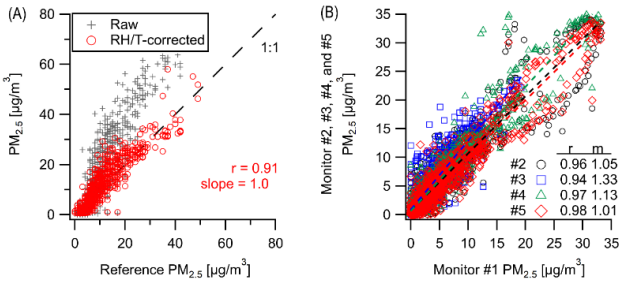

Figure 2: Comparison of $PM_{2.5}$ concentrations between (a) our monitor and the Baltimore Oldtown site reference measurements and (b) an intercomparison of 5 co-located 5 PM sensors over 2.5 weeks in New Haven where there is a high degree of correlation with measurements even at 10-min resolution (time series data can be found in Fig. S8).

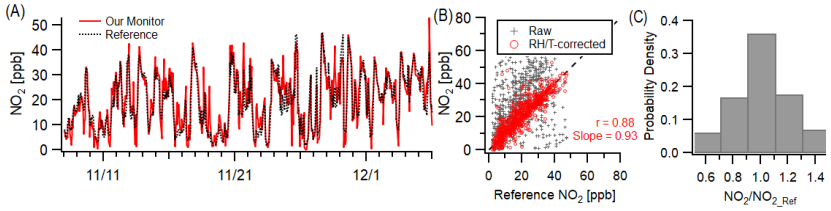

Figure 3: Outdoor ambient monitor comparison of NO_2 from Baltimore, MD (Oldtown site). (a) Time series of ~~environmentally~~RH/T-~~corrected~~ multipollutant monitor data with ~~the~~ reference data. (~~a~~ b) With RH/T correction factors the data achieves good correlation. (c) Over 35% of the measurements are within 10% of the reference site.

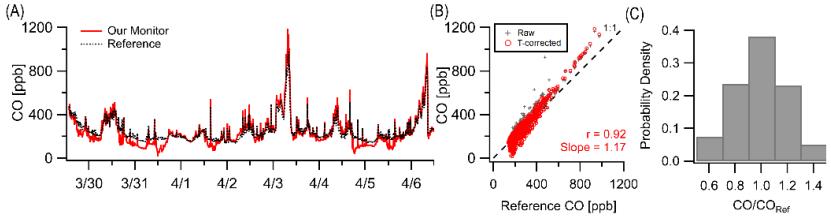

Figure 4: (a) Outdoor ambient monitor comparison of temperature-corrected CO data from New Haven, CT with ~~the~~ reference ~~monitor~~data. (b) Minimal overall effects from RH/T were observed (although the effect of T could be amplified at higher ambient levels, see Fig. S9). (c) At a 10-min resolution 38% of data points within 10% of the reference and 85% within 30%.

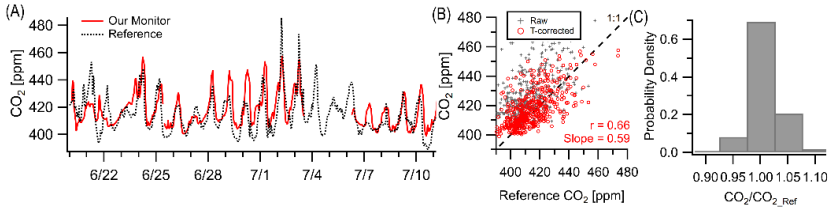

Figure 5: (a–b) Outdoor ambient monitor comparison of temperature-corrected CO_2 data from Baltimore, MD with ~~the~~ reference data. The monitor was located at the OWLETS campaign while the reference data came from the NIST NEB site (2.7 km away). Occasional lags in pollution episodes, potentially due to the displacement of the monitor from the reference, are seen (e.g. 6/30, 7/1, 7/7) leading to a lower correlation coefficient than other pollutants. (c) Despite this, 70% of data points fall within 2.5% of the reference.

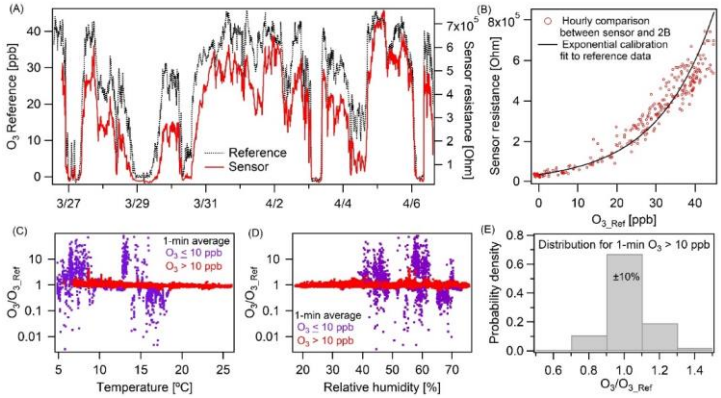

Figure 6: Ozone calibration performance and evaluation (a) over 2 weeks in New Haven, CT shown and (b) calibrated against a 2-B Tech reference monitor (note panel A shows sensor resistance, not concentration). (c-d) The ratio of our calibrated vs. reference measurement for concentrations greater and less than 10 ppb over the range of RH and temperatures observed, with no dependence on RH and a slight temperature dependence. (c–d) At concentrations greater than 10 ppb our measurements are much more accurate, (E) with 70% of the 1 min average data falling within ±10%.

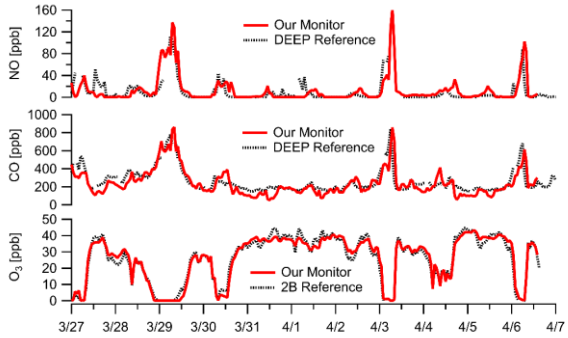

Figure 7: Ambient data at 1 h resolution in New Haven, CT near construction shows large NO enhancements. The presence of NO is confirmed by both the titration of O_3 (i.e. NO+O_3 reaction) to zero and large enhancements in CO (a combustion co-pollutant). The near-road DEEP Criscuolo Park site (1.6 km away from sampling location in downtown New Haven) is used for comparison. Note: our NO sensor does not have significant cross-response to O_3 or CO. (See Fig. S11 for additional NO comparisons.) Multipollutant monitor data is corrected for RH/T where appropriate.

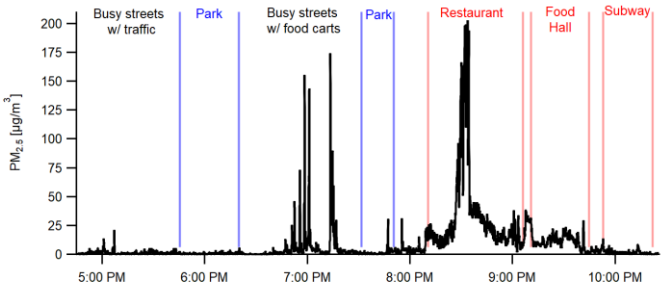

Figure 8: Portable personal monitor data for $PM_{2.5}$ from New York City on June 23rd, 2018 with labeled events, locations, and nearby sources. Data is shown at 1–sec resolution (with RH/T correction factors) capturing rapidly changing microenvironments such as emissions from individual food carts (6:45–7:15 PM).

Formatted: Superscript

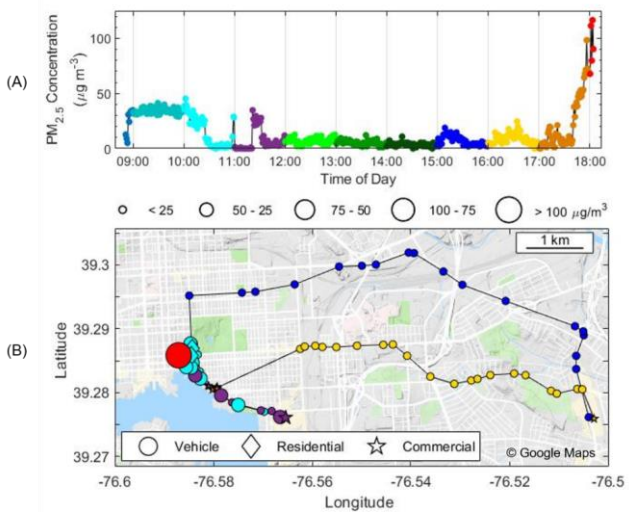

Figure 9: $PM_{2.5}$ mass concentration (µg/m³) as a function of (a) time and (b) mapped with GPS coordinates. The color of the dots in both panels change each hour to represent the time in Panel B. The background colors in Panel A and shapes in Panel B indicates microenvironment, i.e., residential (diamond), commercial (star), and vehicular (circles). The size of the points in (B) corresponds to the mass concentration. This test deployment occurred on March 2nd, 2019.

Formatted: Superscript

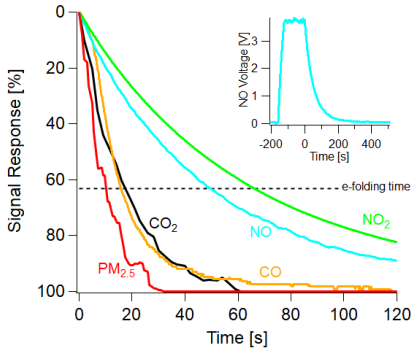

Figure 10: Instrument response times shown as the normalized signal response of various sensors in the stationary monitor to a step change in target pollutant concentration and their respective e-folding times. Insert shows a typical step change of calibration gas and the sensor response. Time zero indicates when the multipollutant monitor switched to sampling zero air after reaching a steady state response to the pollutant. Gas sensor response times vary due to the individual sensors' diffusive or electrochemical timescales.

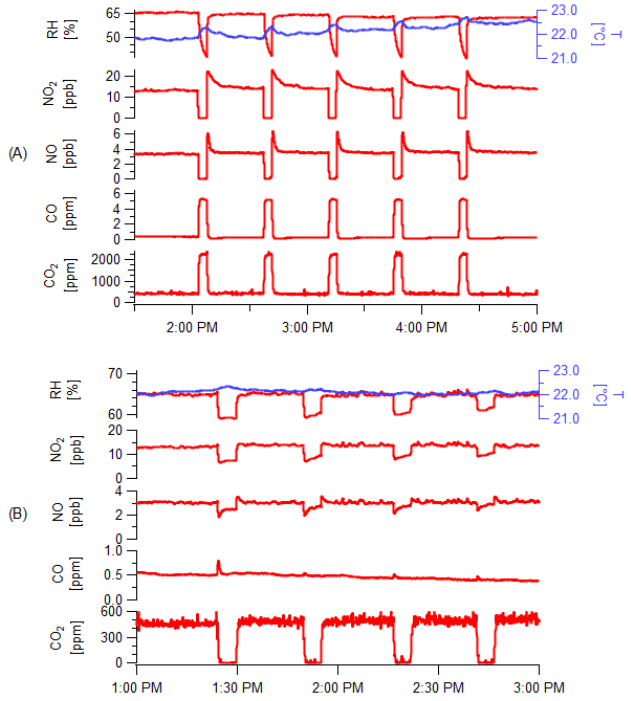

Figure 11: Performance of the on-board calibration system over sequential cycles (for demonstration) showing (a) the span gas delivery for CO and CO_2 (and zero air to provide zero concentrations for NO and NO_2) over 5 repeated cycles and (b) the zeroing function for CO_2 over 4 cycles where other signals are shown to illustrate minimal changes with zero trap (NO_x changes are due to shown RH changes). PM zeroing function results are shown in Fig. S13.

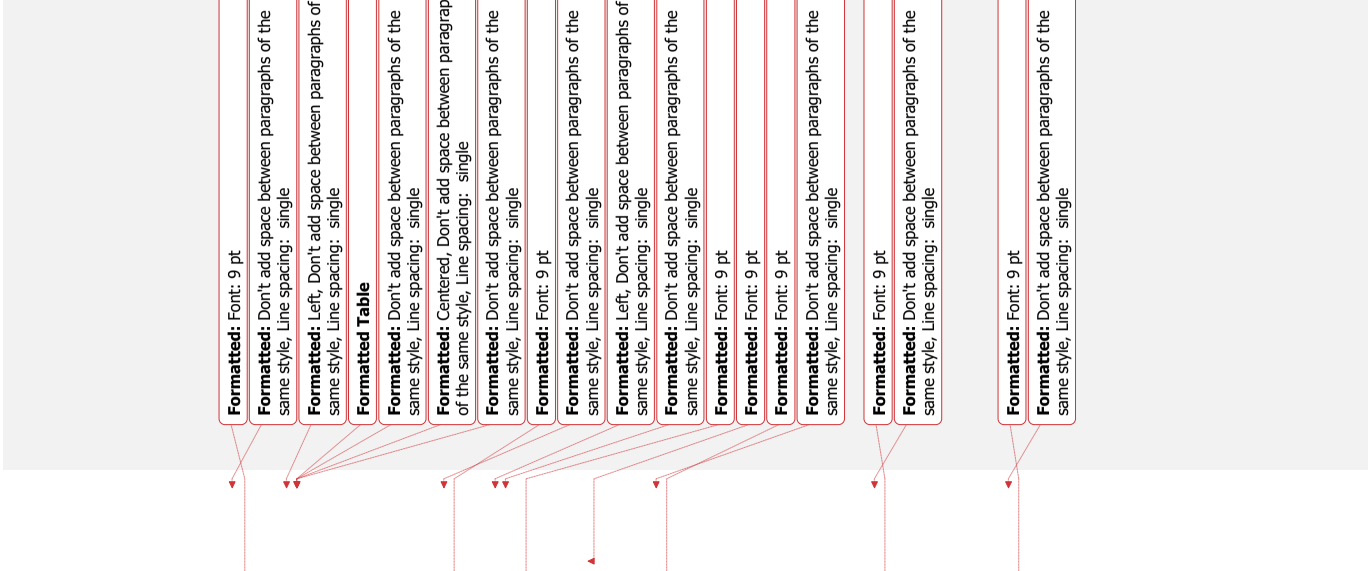

Table 3. Summary of statistics and comparison of the SEARCH stationary multipollutant monitor to several recent literature field studies (NO_2, NO, and CO).

Pollutant	Sensor Type	Temp. Res.	Deployment Length	Deployment Location	Unit	m	r	r^2	MBE	MAE	RMSE	Reference
NO_2	Alphasense NO2-B4	10 min	4 months	Zurich-Kaserne, Switzerland	ppb			0.80		5.8	8.3	Bigi et al., 2018[b]
	Alphasense NO2-B43F	15 min	24 days	Pittsburgh, PA	ppb	0.64		0.67	-0.4	3.48		Zimmerman et al., 2018
	Alphasense NO2-B43F	5 min	89 days	Boston, MA	ppb	0.81		0.69	1.2	3.45	4.56	Cross et al., 2017
	Alphasense NO2-B4	15 min	3 months	Oslo, Norway	ppb	0.38[a]	0.49		13.3	26.23	30.27	Castell et al., 2017
	Alphasense NO2-B42F/B43F	1 hr	1 week	Oakland, CA	ppb		0.61			4.12		Kim et al., 2018
	Alphasense NO2-A43F	**1 hr**	**4 weeks**	**Baltimore, MD**	**ppb**	**0.93**	**0.88**	**0.77**	**0.8**	**3.7**	**5.3**	**This work**
NO	Alphasense NO-B4	10 min	4 months	Zurich-Kaserne, Switzerland	ppb			0.94		2.26	3.54	Bigi et al., 2018[b]
	Alphasense NO-B4	5 min		Boston, MA	ppb	0.94		0.84	0.97	2.83	4.52	Cross et al., 2017
	Alphasense NO-B4	15 min	3 months	Oslo, Norway	ppb	0.93[a]		0.86	-0.54	12.48	16.35	Castell et al., 2017
	Alphasense NO-B4	1 hr	1 week	Oakland, CA	ppb		0.88			3.63		Kim et al., 2018
	Alphasense NO-A4	**1 hr**	**2 weeks**	**New Haven, CT**	**ppb**	**0.86**	**0.74**	**0.54**	**1.6**	**8.5**	**16**	**This work**
CO	Alphasense CO-B4	15 min	41 days	Pittsburgh, PA	ppb	0.86		0.91	0.1	38		Zimmerman et al., 2018
	Alphasense CO-B4	5 min	75 days	Boston, MA	ppb	0.94		0.88	-10.4	24.8	32.9	Cross et al., 2017
	Alphasense CO-B4	15 min	3 months	Oslo, Norway	ppb	0.88[a]	0.6		-147.21	149.35	170.99	Castell et al., 2017
	Alphasense CO-B4	1 hr	1 week	Oakland, CA	ppb		0.74			50.93		Kim et al., 2018
	Alphasense CO-A4	**10 min**	**1 week**	**New Haven, CT**	**ppb**	**1.2**	**0.92**	**0.84**	**5**	**41**	**59**	**This work**
	Alphasense CO-A4	**1 hr**	**1 week**	**New Haven, CT**	**ppb**	**1.2**	**0.96**	**0.92**	**6**	**33**	**43**	**This work**

[a] Slope and intercept value from unit 688150 in Table 2. [b] Taken from Fig. 11 from SU009.

Table 4. Summary of statistics and comparison of the SEARCH stationary multipollutant monitor to several recent literature field studies (CO_2, O_3, and $PM_{2.5}$).

Pollutant	Sensor Type	Temp. Res.	Deployment Length	Deployment Location	Unit	m	r	r^2	MBE	MAE	RMSE	Reference
CO_2	Gascard NG & S-100H	1 hr	85-87 days	Ispra, Italy	ppm	0.48-0.67		0.51-0.79				Spinelle et al., 2017[b]
	Vaisala CarboCap GMP343	1 min	2 weeks	Oakland, CA	-			0.999				Shusterman et al., 2016
	Alphasense IRC-A1	**1 hr**	**3 weeks**	**Baltimore, MD**	**ppm**	**0.59**	**0.66**	**0.44**	**3.4**	**8.7**	**11**	**This work**
O_3	Alphasense Ox-B431	15 min	38 days	Pittsburgh, PA	ppb	0.82		0.86	-0.14	3.36		Zimmerman et al., 2018
	Alphasense Ox-B421	5 min	87 days	Boston, MA	ppb	0.47		0.39	6.78	7.34	9.71	Cross et al., 2017
	Alphasense Ox-B421	15 min	3 months	Oslo, Norway	ppb	0.26[a]	0.54		6.76	19.87	22.2	Castell et al., 2017
	Alphasense Ox-B431	1 hr	5 months	Piacenza, Italy	ppb	0.89		0.88				Ripoll et al., 2019
	MiCS-2614	1 hr	5 months	Piacenza, Italy	ppb	0.90		0.89				Ripoll et al., 2019
	Alphasense Ox-B431/B421	1 hr	1 week	Oakland, CA	ppb		0.69			5.04		Kim et al., 2018
	MiCS-2614	**1 min**	**1.5 weeks**	**New Haven, CT**	**ppb**	**0.99**	**0.97**	**0.94**	**-0.2**	**2.7**	**3.3**	**This work**
	MiCS-2614	**1 hr**	**1.5 weeks**	**New Haven, CT**	**ppb**	**1.01**	**0.98**	**0.96**	**-0.2**	**2.4**	**2.9**	**This work**
$PM_{2.5}$	TSI AirAssure	1 hr	8 weeks	Riverside, CA	$\mu g/m^3$	1.06		0.73	3.9	5.6	7.8	Feenstra et al., 2019[c]
	SainSmart P3 Plantower PMS5003	1 hr	8 weeks	Riverside, CA	$\mu g/m^3$	1.48		0.76	3.9	5.4	7.8	Feenstra et al., 2019[c]
	Aeroqual AQY Nova SDS011	1 hr	8 weeks	Riverside, CA	$\mu g/m^3$	0.98		0.79	-3.1	4.6	6.1	Feenstra et al., 2019[c]
	Shinyei PM Eval. Kit PPD71	1 hr	8 weeks	Riverside, CA	$\mu g/m^3$	1.11		0.74	0.2	4.4	6.4	Feenstra et al., 2019[c]
	PurpleAir PA-II Plantower PMS5003	1 hr	8 weeks	Riverside, CA	$\mu g/m^3$	1.53		0.95	4.8	6.8	10.1	Feenstra et al., 2019[c]
	AQMesh OPC v3.0	15 min	3 months	Oslo, Norway	$\mu g/m^3$		0.51		-0.03	3.08	5.57	Castell et al., 2017
	Plantower A003	**1 hr**	**2 weeks**	**Baltimore, MD**	**$\mu g/m^3$**	**1.0**	**0.91**	**0.82**	**0.9**	**3.1**	**4.3**	**This work**

[a] Slope and intercept value from unit 688150 in Table 2. [b] From correlation using an Artifical Neural Network calibration. [c] Top five performing (by r^2) monitors.

Formatted: Left Formatted: Left Formatted: Left Formatted: Left Formatted: Left Formatted: Left

Table 3. Summary of statistics and comparison of the SEARCH stationary multipollutant moni tor to several recent literature field studies.

Pollutant	Sensor Type	Temp. Res.	Unit	m	r	r^2	MBE	MAE	RMSE	Reference
NO_2	Alphasense NO2-B4	10 min	ppb			0.80		5.8	8.3	Bigi et al., 2018[d]
	Alphasense NO2-B43F	15 min	ppb	0.64		0.67	-0.4	3.48		Zimmerman et al., 2018
	Alphasense NO2-B43F	5 min	ppb	0.81		0.69	1.2	3.45	4.56	Cross et al., 2017
	Alphasense NO2-B4	15 min	ppb	0.38[a]	0.49		13.3	26.23	30.27	Castell et al., 2017
	Alphasense NO2-A43F	**1 hr**	**ppb**	**0.93**	**0.88**	**0.77**	**0.8**	**3.7**	**5.3**	**This work**
NO	Alphasense NO-B4	10 min	ppb			0.94		2.26	3.54	Bigi et al., 2018[d]
	Alphasense NO-B4	5 min	ppb	0.94		0.84	0.97	2.83	4.52	Cross et al., 2017
	Alphasense NO-B4	15 min	ppb	0.93[a]		0.86	-0.54	12.48	16.35	Castell et al., 2017
	Alphasense NO-A4	**1 hr**	**ppb**	**0.86**	**0.74**	**0.54**	**1.6**	**8.5**	**16**	**This work**
CO	Alphasense CO-B4	15 min	ppb	0.86		0.91	0.1	38		Zimmerman et al., 2018
	Alphasense CO-B4	5 min	ppb	0.94		0.88	-10.4	24.8	32.9	Cross et al., 2017
	Alphasense CO-B4	15 min	ppb	0.88[a]	0.6		-147.21	149.35	170.99	Castell et al., 2017
	Alphasense CO-A4	**10 min**	**ppb**	**1.2**	**0.92**	**0.84**	**5**	**41**	**59**	**This work**
	Alphasense CO-A4	**1 hr**	**ppb**	**1.2**	**0.96**	**0.92**	**6**	**33**	**43**	**This work**
CO_2	Gascard NG & S-100H	1 hr	ppm	0.48-0.67		0.51-0.79				Spinelle et al., 2017[b]
	Alphasense IRC-A1	**1 hr**	**ppm**	**0.59**	**0.66**	**0.44**	**3.4**	**8.7**	**11**	**This work**
O_3	Alphasense Ox-B431	15 min	ppb	0.82		0.86	-0.14	3.36		Zimmerman et al., 2018
	Alphasense Ox-B421	5 min	ppb	0.47		0.39	0.78	7.34	9.71	Cross et al., 2017
	Alphasense Ox-B421	15 min	ppb	0.26[a]	0.54		6.76	19.87	22.2	Castell et al., 2017
	Alphasense Ox-B431	1 hr	ppb	0.91		0.89				Ripoll et al., 2019
	MiCS-2614	1 hr	ppb	0.87		0.88				Ripoll et al., 2019
	MiCS-2614	**1 min**	**ppb**	**0.99**	**0.97**	**0.94**	**-0.2**	**2.7**	**3.3**	**This work**
	MiCS-2614	**1 hr**	**ppb**	**1.01**	**0.98**	**0.96**	**-0.2**	**2.4**	**2.9**	**This work**
$PM_{2.5}$	TSI AirAssure	1 hr	$\mu g/m^3$	1.06		0.73	3.9	5.6	7.8	Feenstra et al., 2019[c]
	SainSmart P3 Plantower PMS5003	1 hr	$\mu g/m^3$	1.48		0.76	3.9	5.4	7.8	Feenstra et al., 2019[c]
	Aeroqual AQY Nova SDS011	1 hr	$\mu g/m^3$	0.98		0.79	-3.1	4.6	6.1	Feenstra et al., 2019[c]
	Shinyei PM Eval. Kit PPD71	1 hr	$\mu g/m^3$	1.11		0.74	0.2	4.4	6.4	Feenstra et al., 2019[c]
	PurpleAir -PA-II Plantower PMS5003	1 hr	$\mu g/m^3$	1.63		0.95	4.8	6.8	10.1	Feenstra et al., 2019[c]
	AQMesh OPC v3.0	15 min	$\mu g/m^3$		0.51		-0.03	3.08	5.57	Castell et al., 2017
	Plantower A003	**1 hr**	**$\mu g/m^3$**	**1.0**	**0.91**	**0.82**	**0.9**	**3.1**	**4.3**	**This work**

Supporting Information for:

Stationary and Portable Multipollutant Monitors for High Spatiotemporal Resolution Air Quality Studies including Online Calibration

Colby Buehler[1,2], Fulizi Xiong[1,2], Misti Levy Zamora[2,3], Kate M. Skog[1], Joseph Kohrman-Glaser[4], Stefan Colton[4], Michael McNamara[5], Kevin Ryan[5], Carrie Redlich[6,7], Matthew Bartos[8], Brandon Wong[8], Branko Kerkez[8], Kirsten Koehler[2,3], Drew R. Gentner[1,2,9,*]

[1] Department of Chemical & Environmental Engineering, Yale University, School of Engineering and Applied Science, New Haven, Connecticut 06511, USA

[2] SEARCH (Solutions for Energy, Air, Climate and Health) Center, Yale University, New Haven, CT, USA

[3] Department of Environmental Health and Engineering, Johns Hopkins Bloomberg School of Public Health, Baltimore, MD, 21205, USA

[4] Department of Mechanical Engineering, Yale University, School of Engineering and Applied Science, New Haven, Connecticut, 06511, USA

[5] Department of Electrical Engineering, Yale University, School of Engineering and Applied Science, New Haven, Connecticut, 06511, USA

[6] Department of Internal Medicine, Yale University, School of Medicine, New Haven, Connecticut, 06510, USA

[7] Department of Environmental Health Sciences, Yale University, School of Public Health, New Haven, Connecticut, 06511, USA

[8] Civil and Environmental Engineering, University of Michigan, 2350 Hayward St, G.G. Brown Building, Ann Arbor, MI 48109, USA

[9] Max Planck Institute for Chemistry, Mainz 55128, Germany.

Correspondence to: Drew R. Gentner (drew.gentner@yale.edu)

Pages: 11

Number of Figures: 14

Number of Tables: 1

Table of Contents: Supporting Figures and Tables

List of Tables

List of Figures

S1 Concentration Conversion Methodology and Example

First, raw voltages are collected and converted to concentrations based on a laboratory derived calibration curve for each box. For the electrochemical sensors, we use the differential voltage, which is the working electrode minus the auxiliary electrode.

$$Volt_{diff} = Volt_{WE} - Volt_{AE}, \quad \text{(S1)}$$

In the case below for this particular monitor there is a linear relationship between the differential voltage and the known concentration of reference gas (see Fig.S1). The fit follows the form of:

$$C_{raw} = a_{cal}\, Volt_{diff} + b_{cal}, \quad \text{(S2)}$$

where C_{raw} represents the non-RH/T corrected concentration value. This fit works well for the Alphasense electrochemical sensors. See notes at the end for CO_2 sensor fits. The limit of detection values shown in Table 1 are calculated by taking three times the standard deviation of the sensor output in zero air and dividing by the slope (a_{cal}).

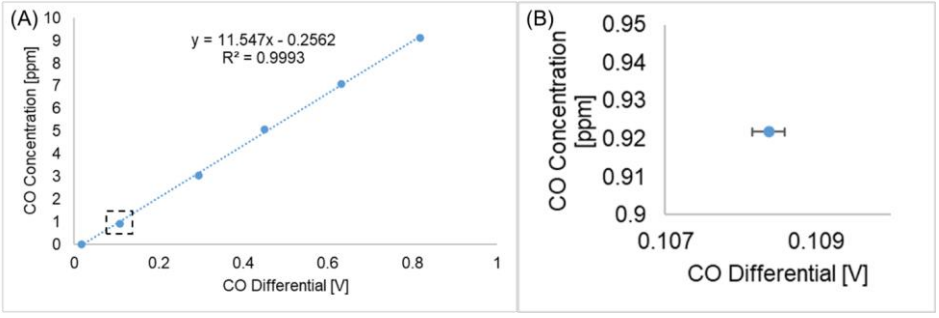

Figure S1: (a) Laboratory linear calibration of one CO sensor under a range of known gas concentrations and (b) zoom in on one point to show minimal standard deviation in differential signal for a several minute period under constant laboratory RH/T setting.

For this study we implement RH/T correction factors from co-location evaluations rather than from lab calibrations. Using a training period, we apply the following equations to reach a final concentration:

$$C_T = \frac{C_{raw}}{a_T T^2 + b_T T + c_T}, \quad \text{(S3)}$$

$$C_{RH/T} = \frac{C_T}{a_{RH} RH^2 + b_{RH} RH + c_{RH}}, \quad \text{(S4)}$$

First the ratio of the monitor value over the reference is plotted against temperature. We apply a best-fit linear and quadratic regression to determine the relationship (see Fig. S2). Then we examine the r^2 value for each and choose the fit with the strongest correlation. Here, the best temperature relationship is determined to be quadratic (apply fit to Eqn. S2 to extract temperature corrected concentration). Then the temperature corrected concentration relative to reference is plotted against

relative humidity. Here, the best relative humidity relationship is linear (apply fit to Eqn. S3 to extract the final concentration data). With these two relationships we can apply the RH/T correction factors to the rest of the data.

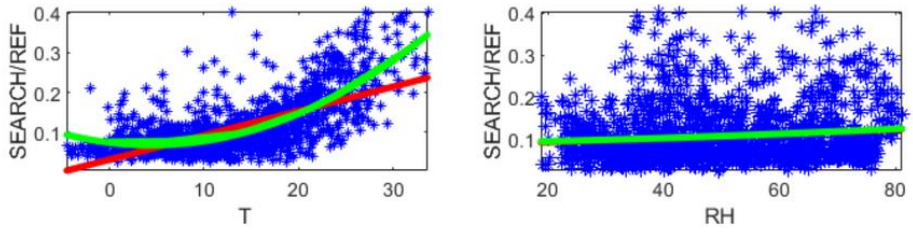

Figure S2: Training period example for the NO_2 sensor after a one-week co-location. The left shows the ratio of the multipollutant monitor concentration relative to the reference monitor against T. The right shows the ratio of the temperature corrected multipollutant monitor concentration relative to the reference against RH. These plots are used to generate the coefficients for the denominators of Eqn S3 and Eqn S4.

Notes for CO_2: The CO_2 calibrations follows Alphasense technical documentation rather than the above methodology (Alphasense Ltd., 2014). No RH adjustment is made for the CO_2 sensor, only the Alphasense-specified T correction. In addition, when aggregating the data to evaluate the CO_2 sensor relative to a reference, we implement a rolling geometric mean rather than arithmetic for averaging and smoothing sensor response. All other sensors use an arithmetic mean for calculations.

S2 Comparison with Literature

In a systematic review of the literature, Karagulian et al. (2019) compiled the r^2 and slope values of numerous field and laboratory co-locations for low cost monitors. They then determined a "best selection region" for monitors from the union of high correlation ($r^2>0.75$) and minimal over or under estimation ($0.5<m<1.5$). Three out of our five co-located pollutants (O_3, CO, $PM_{2.5}$) discussed in detail lie inside of the best selection region, with one additional pollutant (NO_2) along the edge (Fig. S12). Two pollutants do not fall near this region (CO_2 and NO) for reasons previously discussed in the main text.

References:

Alphasense Ltd.: AAN 201-06 NDIR: Gas Concentration Calculation Overview, [online] Available from: http://www.alphasense.com/WEB1213/wp-content/uploads/2014/12/AAN_201-06.pdf, 2014.

Karagulian, F., Barbiere, M., Kotsev, A., Spinelle, L., Gerboles, M., Lagler, F., Redon, N., Crunaire, S. and Borowiak, A.: Review of the performance of low-cost sensors for air quality monitoring, Atmosphere (Basel)., 10(9), doi:10.3390/atmos10090506, 2019.

Table S1: Physical and electronic technical information on the stationary and portable monitors.

	Stationary	Portable
Dimensions (cm)	28 x 18 x 14	15 x 6.5 x 5[1] 23 x 12 x 6.5[2]
Power	Wall Outlet	Tenergy #31800 Rechargable Li-ion Battery (11.1 V 10.4 Ah, 115.45 Wh)
Data Storage	Onboard 16 GB SanDisk Edge MicroSD	
Data Transmission	Cellular communication to InfluxDB via Telit LE910C1-NS module at 10s interval	N/A
Microcontroller	Cypress 68 pin PSoC 5lp	
Software	PSoC Creator 4.1	
Cell Antenna	LTE + Cellular flexiiANT Mitis SRFL026	N/A
GPS Antenna	N/A	Octaband LTE Cellular Embedded antenna (FPC) 1002292
Operational Duration	Indefinitely	~3 days per single charge

[1]Dimensions for shoulder mountable sensor manifold and enclosure

[2]Dimensions for motherboard enclosure and battery

105

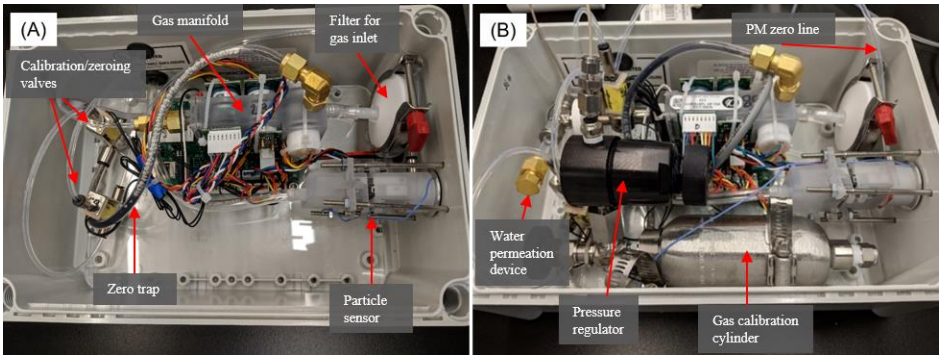

Figure S3: Photo of the (A) non-cylinder and (B) cylinder version of the stationary multipollutant monitor.

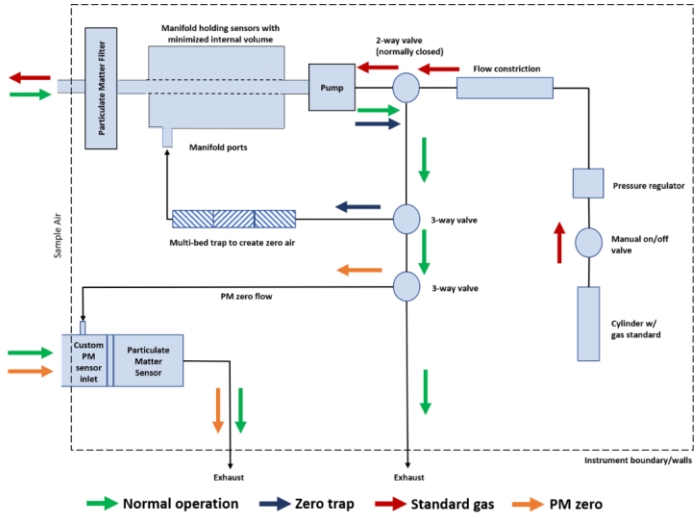

Figure S4: Calibration system flow diagram in the overall system schematic for Yale multipollutant monitor. This system includes calibration approaches for both the gas-phase sensors and particulate matter sensor. The pump operates during all sampling modes except when the standard gas cylinder is used.

(A)

(B)

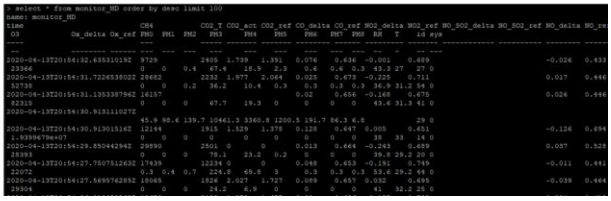

Figure S5: Data management and visualization software to see real time measurements. Grafana (A) is an open source data visualization platform allowing us to interface directly with our data management software InfluxDB (B) which is accessed through the secure shell PuTTY.

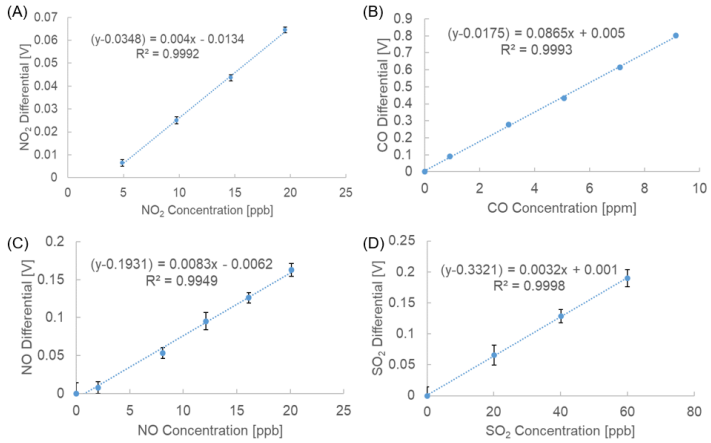

Figure S6: Demonstration of linearity of electrochemical sensor calibration. Error bars represent standard deviation of signal over several minutes of exposure to the target gas at a given concentration. Note that this is for the calibration of one sensor and there is variation in slopes among sensors.

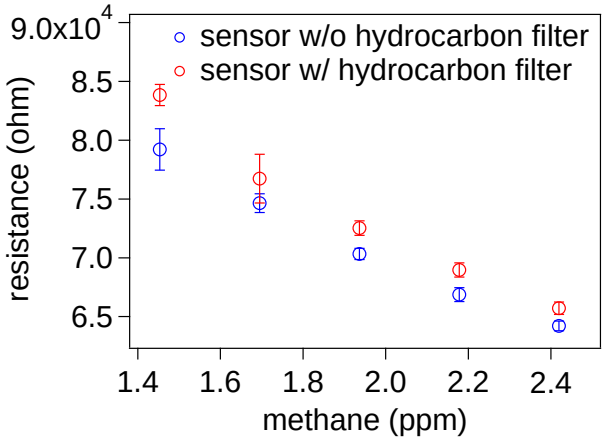

Figure S7: Calibration data for the Figaro TGS 2600 CH_4 sensor. A linear response is observed in typical ambient or urban background levels both with and without an activated carbon cloth filter to remove cross-sensitivity to VOCs.

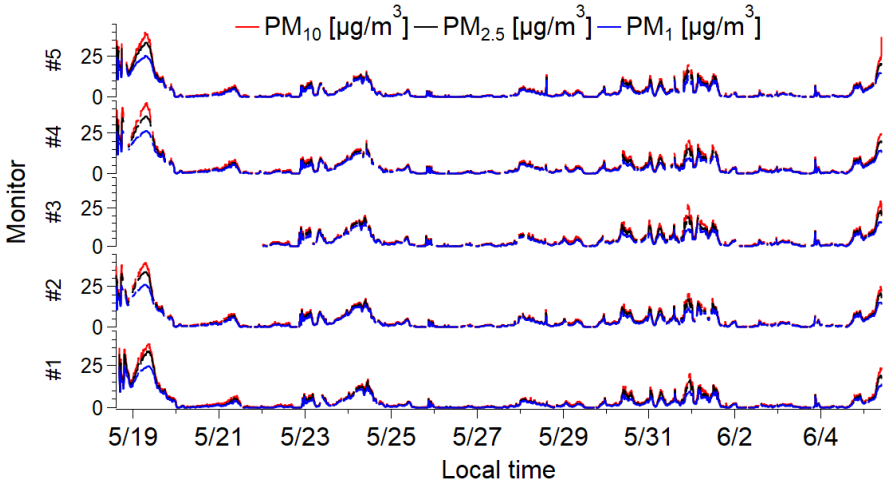

Figure S8: PM sensor intercomparison (raw data) for 5 co-located monitors over 2.5 weeks in New Haven, CT (accompanies data shown in Fig. 2b).

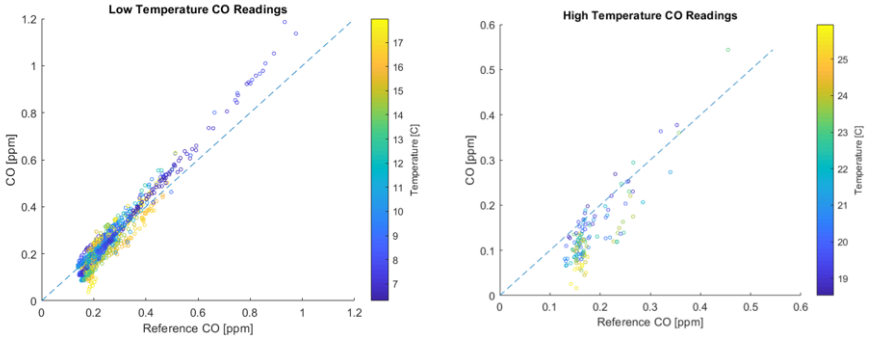

Figure S9: CO comparisons to reference instrument for low (<18 °C, left) and high (>18 °C, right) temperature readings. This accompanies Fig. 4 in the main text.

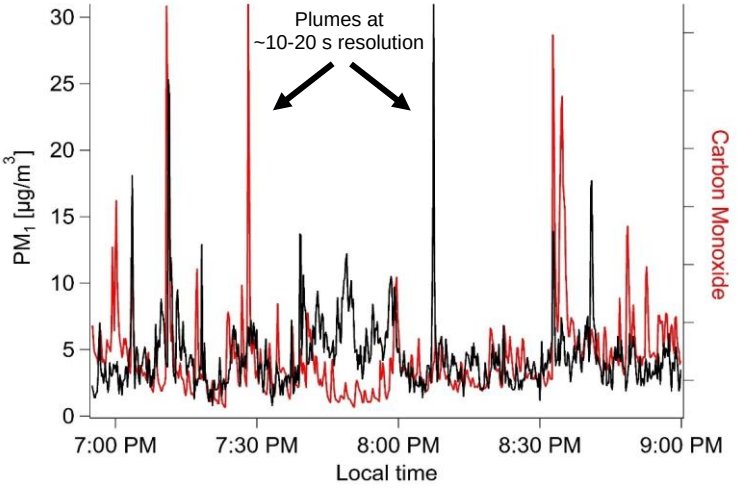

Figure S10: Additional examples of field data with fast monitor response times to concentration changes demonstrated roadside with motor vehicle spikes in PM_1 and raw CO differential signal at 10-s resolution.

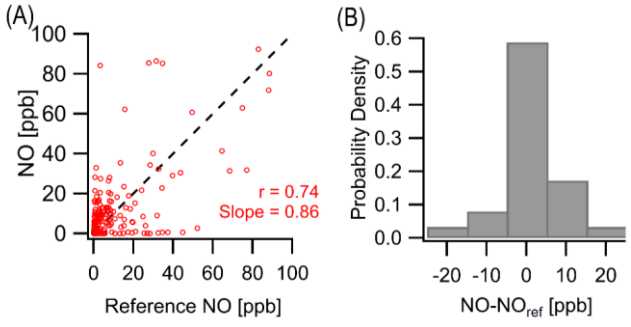

Figure S11: NO sensor regression (A) and probability density (B) from a two-week field deployment in New Haven, CT. The reference instrument comes from the near-road DEEP Criscuolo Park site (1.6 km away from sampling location in downtown New Haven). Given the generally low NO levels during the sampling period the probability density is shown as the MBE rather than the ratio of sensor to reference as in main text figures. Nearly 60% of data points fall within ±5 ppb of the reference at a 1 h resolution. Accompanies the data shown in Fig. 7.

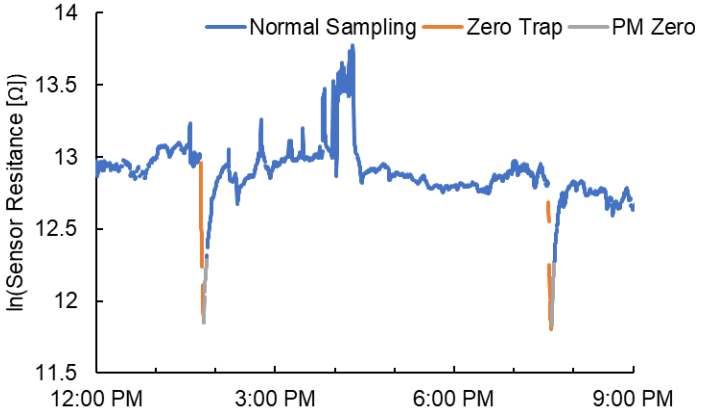

Figure S12: Performance of the zero trap for O_3 removal via steel wool and activated carbon shown as raw O_3 sensor resistances. Two tests during a mid-July afternoon in Baltimore, MD show a rapid decrease in sensor response through the zero trap (orange) relative to normal sampling and other calibration steps. Note: data are shown on a logarithmic scale due exponential response to concentration.

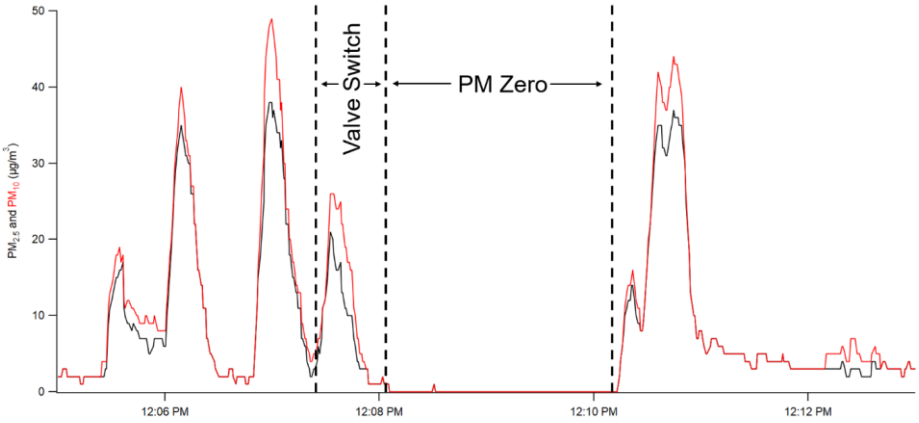

Figure S13: Raw $PM_{2.5}$ (black) and PM_{10} (red) sensor zero near food-cooking carts in New Haven, CT. After the valve switch, a short lag occurs (i.e. to purge inlet) before the sensor is zeroed for two minutes.

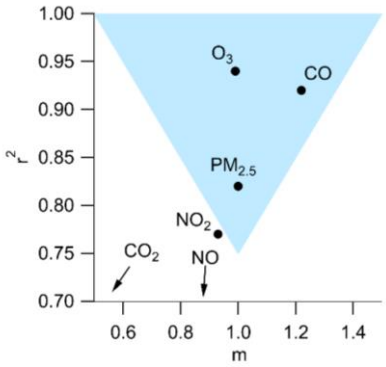

Figure S14: Sensor r^2 and slope values for collocation data. Blue shaded triangle represents the "best selection region" from Karagulian et al. (2019). Three of our measurements lie within this region (O_3, CO, and $PM_{2.5}$), with one along the edge (NO_2). Two pollutants (CO_2 and NO) did not fall into the region partially due to not having a true co-location comparison (reference sites were 2.7 and 1.6 km away from sampling location, respectively).

Formatted: Left, Line spacing: single